AD-A271 209

(2)

Revised
10-01-93

Microtribology of Magnetic Media

Bharat Bhushan, Vilas N. Koinkar and Ju-Ai Ruan
Computer Microtribology and Contamination Laboratory
Department of Mechanical Engineering
The Ohio State University
Columbus, OH 43210-1107, U.S.A.

ONR N00014-93-I-0067

ABSTRACT

Scanning tunneling microscopy (STM), atomic force microscopy (AFM), and the modifications of AFMs [such as friction force microscopy (FFM)] are becoming increasingly important in the understanding of fundamental mechanisms of friction, wear and lubrication and in studying the interfacial phenomena in micro- and nanostructures used in magnetic storage devices and micro-electromechanical systems (MEMS). In this paper, we describe modified AFM and FFM techniques and present data on microtribological studies of magnetic media-magnetic tapes and disks. Local variation in microscale friction is found to correspond to the local slope suggesting that ratchet mechanism is responsible for this variation. Wear rates for magnetic tapes are approximately constant for various loads and test duration. However, for magnetic disks, the wear of the diamondlike carbon overcoat is catastrophic. Evolution of the wear has also been studied using AFM. AFM has been modified for nanoindentation hardness measurements. We have shown that hardness of ultra thin films can be measured using AFM. AFM has also shown to be useful for nanofabrication.

Invited paper for publication in the first issue of Journal of Engineering Tribology, Trans. The Institution of Mechanical Engineers, London.

1.0 INTRODUCTION

The capability of new techniques to measure surface topography, adhesion, friction, wear and lubricant film thickness on a nanometer scale and to image lubricant molecules, and the availability of supercomputers to conduct atomic-scale simulations, have led to the development of a new field referred to as Microtribology, Nanotribology, Molecular Tribology or Atomic-Scale Tribology. This field deals with experimental and theoretical investigations of atomic and molecular processes involved in adhesion, friction, wear, and thin-film boundary lubrication which occur at the sliding interface. Microtribological studies are needed to develop a fundamental understanding of interfacial phenomena and for studying interfacial phenomena in micro-and nano structures used in magnetic storage systems, microelectromechanical systems (MEMS) and other industrial applications. The components used in micro- and nano structures are very light (on the order of a few tens of micrograms) and are operated under very light loads (on the order of a few micrograms to a few milligrams). As a result, friction and wear (nanoscopic wear) of lightly-loaded micro/nano components are highly dependent on the surface interactions (few atomic layers). Microtribological techniques are ideal for studying the friction and wear processes of micro/nano structures. These new instruments can also be used for nanofabrication.

Scanning Tunneling Microscope (STM) developed by Binnig et al. (1) is the first instrument capable of directly obtaining three-dimensional (3D) images of solid surfaces with atomic resolution. In STM, a tunneling current is sensed between a conducting solid and a sharp metal tip (2) held about 0.3-1 nm above the solid surface with an operating voltage of 2mV to 2V. Because the current increases by approximately a factor of 10 for each 0.1 nm the tip is brought closer to the surface, the tunneling current (micro to nano amperes) is a very sensitive measure of the tip-surface distance. To image a sample surface, two piezoelectric drivers raster the tip parallel to the plane of the sample. A feedback loop drives a third piezoelectric element perpendicular to the sample to adjust the tip position to keep the current or tip-surface separation constant. The tip position gives a 3D image of the sample surface.

Based on their design of STM, Binnig et al. (3) developed an Atomic Force Microscope (AFM) [also called Scanning Probe Microscope (SPM)] to measure ultrasmall forces (less than 1μN) present between the AFM tip surface and a sample surface. They measured these small forces by measuring the motion of a cantilever beam having an ultrasmall mass. While STM requires that the surface to be measured be electrically conductive, AFM is capable of investigating surfaces of both conductors and insulators on an atomic scale if suitable techniques for measurement of cantilever motion are used. In the operation of high resolution AFM, the sample is generally scanned instead of the tip as in STM, because AFM measures the relative displacement between the cantilever surface and reference surface and any cantilever movement would add vibrations. However, AFMs are now available where the tip is scanned and the sample is stationary. As long as AFM is operated in the so-called contact mode, little if any vibration is introduced. AFMs can be used to study *engineering surfaces* in dry and wet conditions as opposed to a surface force apparatus (SFA) which can only be used to study liquid films between atomically-smooth and optically-transparent surfaces (4-7). The scope of this paper is limited to AFM and its modifications.

For imaging surfaces, AFM can be thought of as a nanometer scale profiler. A sharp tip at the end of a cantilever (8) is brought in contact with a sample surface by moving the sample with piezoelectric transducers. During initial contact, the atoms at the end of the tip experience a very weak repulsive force due to electronic orbital overlap with the atoms in the sample surface. The force acting on the tip causes a lever deflection which is measured by tunneling (3), capacitive (9), or optical detectors such as laser interferometry (10, 11). The optical techniques are believed to be reliable and easily implementable detection methods. The deflection can be measured to within ± 0.02 nm, so for a typical lever force constant of 10 N/m a force as low as 0.2 nN (corresponding normal pressure ~1MPa for a tip radius of about 50 nm) could be detected. This operational mode is referred to as "repulsive mode" or "contact mode" (**3**). An alternative is to use "attractive force imaging" or "non-contact imaging", in which the tip is brought in close proximity (within a few nm) to, and not in contact with the sample (**12**). Very weak Van der Waals attractive force is present at the tip-sample interface. Although in this technique the normal pressure exerted at the interface is zero (desirable to avoid any surface deformation), it is slow, difficult to use and has poor resolution, and is rarely used outside research environments. In either mode, surface topography is generated by laterally scanning the sample under the tip while simultaneously measuring the separation-dependent force or force gradient (derivative) between the tip and the surface. The force gradient is obtained by vibrating the cantilever and measuring the shift of resonance frequency of the cantilever (**12**). To obtain topographic information, the interaction force is either recorded directly, or used as a control parameter for a feedback circuit that maintains the force or force derivative at a constant value. Force derivative is normally tracked in non-contact imaging. With AFM operated in the contact mode, topographic images with a vertical resolution of less than 0.1 nm (as low as 0.01 nm) and a lateral resolution of about 0.2 nm have been obtained (**13-15**). With a 0.01 nm displacement sensitivity, 10 nN to 1 pN forces are measurable. These forces are comparable to the forces associated with chemical bonding, e.g., 0.1 μN for an ionic bond and 10 pN for a hydrogen bond (**3**).

To minimize friction effects in the topography measurements in the contact-mode AFMs and to measure topography of soft surfaces, AFMs can be operated in the so called "force modulation mode" or "tapping mode" (**16, 17**). In the force modulation mode, the tip is lifted and then lowered to contact the sample (oscillated at a constant amplitude) during scanning over the surface with a feedback loop keeping the average force constant. This technique eliminates frictional force entirely. The tip is oscillated at about 300 kHz with a 20-100 nm amplitude introduced in the vertical direction. The amplitude is kept large enough so that the tip does not get stuck to the sample because of adhesive attractions. The force modulation mode can also be used to measure local variations in surface mechanical properties.

An important property of AFM is its ability to go beyond topographic measurements (**18-20**) and to investigate different phenomena (**21**) such as magnetism (magnetic force measurements including its application for magnetic recording) (**22-24**), electrostatic attraction, chemical interaction (**25**), adhesion (**26-28**), friction and wear (**10, 29-32**), material manipulation (**33**), and thin-film boundary lubrication (**34-39**), to image lubricant molecules (**40, 41**), to measure surface temperatures (**42**), and to measure surface mechanical properties such as hardness and modulus of elasticity (**16, 17, 43**). STMs and AFMs have also been used for nanofabrication (**44, 45**).

Mate et al. (**10**) were the first to modify an AFM in order to measure both normal and friction forces and this instrument is generally called "Friction Force Microscope" (FFM) or "Lateral Force Microscope" (LFM). They measured atomic-scale friction of a tungsten tip sliding on a basal plane of a single grain of highly-oriented pyrolytic graphite (HOPG). Since then several research groups have developed various designs of FFMs. As stated earlier, modifications to AFM have also been made to study other phenomena. There are a number of manufacturers who produce commercial AFM/FFM instruments with scanning lengths ranging from about 0.7 μm (for atomic resolution) to about 100 μm or larger.

In this paper, we describe atomic force microscopy and its modifications developed for microtribological studies to conduct friction, scratching, wear, indentation, and lubrication studies, and its applications for nanofabrication. We also present the status of microtribology of magnetic media.

2.0 DESCRIPTION OF AFM / FFM AND MEASUREMENT TECHNIQUES

We used a modified commercial AFM/FFM (Nanoscope III from Digital Instruments, Inc., Santa Barbara, CA), Fig. 1, to conduct studies of friction, scratching, wear, indentation, lubrication and nanofabrication (**31, 32, 46**). Simultaneous measurements of friction force and surface roughness can be made using this instrument. The sample is mounted on a piezoelectric tube (PZT) scanner which can precisely scan the sample in the horizontal (x-y) plane and can move the sample in the vertical (z) direction. A sharp tip at the free end of a cantilever is brought in contact with the sample. A laser beam from a laser diode is focused onto the back of a cantilever near its free end. The cantilever is tilted downward at about 10^0 with respect to the horizontal plane. The beam is reflected from the cantilever and is directed through a mirror onto a split photodetector with four quadrants. Two quadrants (top and bottom) of the detector are used for topography measurements. As the sample is scanned under the tip, topographic features of the sample cause the tip to deflect in vertical direction. This tip deflection will change the direction of the reflected laser beam, changing the intensity difference between the top and bottom photodetector (AFM signal). For topographic imaging or for any other operation in which the applied normal force is to be kept a constant, a feedback circuit is used to modulate the voltage applied to the PZT scanner to adjust the height of the PZT, so that the cantilever vertical deflection (given by the intensity difference between the top and bottom detector) will remain almost constant during scanning. The PZT height variation is thus a direct measure of surface roughness of the sample.

Microfabricated Si_3N_4 tips are used for topographic imaging, friction force measurements, and for nanowear and nanoindentation studies at very light loads (about 100 nN or less). Si_3N_4 cantilever beams with integrated square pyramidal tips with a tip radius of about 30-50 nm are produced by plasma-enhanced chemical-vapor-deposition (PECVD) (Figs. 2a and 2b, top). The normal spring stiffness of these beams ranges from 0.06 to 0.58 N/m. Single-crystal natural diamond tips are used for nanowear, nanoscratch and nanoindentation measurements at relatively higher loads (1μN to 100 μN). The tips are ground to the shape of a three-sided pyramid with an apex angle of 80^0 whose point is sharpened to a radius of about 100 nm (Figs. 2a and 2b, bottom). The tips are bonded with conductive epoxy to a gold-plated 304 stainless steel spring sheet (length= 20 mm, width= 0.2 mm, thickness= 20 to 60 μm) which acts as a cantilever. Free length of the spring is varied to change the beam stiffness. The normal stiffness of the beam ranges from about 5 to 600 N/m for a 20 μm thick beam.

For measurement of friction force being applied at the tip surface during sliding, the other two (left and right) quadrants of the photodetector (arranged horizontally) are used. The sample is scanned back and forth in a direction orthogonal to the long axis of the cantilever beam. Friction force between the sample and the tip will produce a twisting of the cantilever. As a result, the laser beam will be reflected out of the plane defined by the incident beam and the beam reflected vertically from an untwisted cantilever. This produces an intensity difference of the laser beam received in the left and right quadrants of the photodetector. The intensity difference between the left and right detectors (FFM signal) is directly related to the degree of twisting, hence to the magnitude of friction force. One problem associated with this method is that any misalignment between the laser beam and the photodetector axis would introduce error in the measurement. However, by following the procedures developed by Ruan and Bhushan (31), in which the average FFM signal as the sample is scanned in two opposite directions is subtracted from the friction profiles of each scan, the misalignment effect can be eliminated. By following the normal force and friction force calibration procedures developed by Ruan and Bhushan (31), voltages corresponding to normal and friction forces can be converted to force units. By making measurements at various normal loads, average value of coefficient of friction is obtained which then can be used to convert the friction profile to the coefficient of friction profile. Thus, any directionality and local variation of friction can be measured. Surface topography data can be measured simultaneously with the friction data and local relationship between the two profiles can be established.

Topography measurements were typically made using Si_3N_4 tip (normal cantilever stiffness = 0.4 N/m) at a normal load of 10 nN and friction measurements were carried out in the load range of 10 nN to 100 nN. The tip was scanned in a way that its trajectory on the sample formed a triangular pattern (Fig.3) with a typical scanning speed of 25 nm/s in the fast scan direction and 0.2 nm/s in the perpendicular direction for a 40 nm x 40 nm area. Speed was increased accordingly for larger area scans (200 nm x 200 nm). 256 x 256 data points were taken for each image. The uncertainty associated with the average coefficient of friction was within about ±15%.

In nanoscratch/nanowear studies, a diamond tip was used. Typical normal load used for the scratch and wear ranged from 10 μN to 100 μN with a cantilever stiffness of about 25 N/m. For wear, the scanning speed was 1 μm/s in the fast scan direction and 4 nm/s in the slow scan direction and an area of 2μm x 2 μm was scanned. Sample surfaces were scanned before and after the scratch or wear to obtain the initial and the final surface topography at a load of about 0.5 μN, over an area larger than the scratched or worn region to observe the scratch or wear scars. Additional scratching or wear may have occurred during these scans, but this scratching or wear is much smaller than that generated at higher loads (>10 μN) and is not of the concern.

Nanoindentation studies were conducted in the load range of 10 μN to 140 μN, using the same diamond tip used for nanoscratch/wear studies. The operation procedures for nanoindentation were similar to those used for nanowear except that the scan size was set to zero in the case of nanoindentation, in order for the tip to continuously press the sample surface for about two seconds. Indentation marks were generated on the sample surface as a result of the normal load being applied by the tip. The surface was imaged before and after the indentation at a normal load of about 0.5 μN. Nanohardness was calculated by dividing the indentation load by the projected residual area.

Nanofabrication was performed on a (100) single-crystal silicon wafer by scratching the sample surface with a diamond tip at specified locations and scratching angles. The normal load used for the scratching (writing) was 40 μN and the writing speed was 500 nm/s.

3.0 TEST SAMPLES

For the present study, one magnetic tape and four magnetic thin-film rigid disks were selected (**32**). The tape was a 12.7-mm wide and 13.2-μm thick (base thickness of 9.8 μm, magnetic coating of 2.9 μm, and back coating of 0.5 μm) calendered single-layered metal-particle (MP) tape with an rms roughness of about 5 nm. Four disks with a polished substrate and with a standard textured substrate, with and without a bonded perfluoropolyether lubricant were selected. These disks were 95-mm in diameter made of Al-Mg alloy substrate (1.3 mm thick) with a 10 to 20-μm thick electroless plated Ni-P coating, 75-nm thick ($Co_{79}Pt_{14}Ni_7$) magnetic coating, 20 to 30-nm thick diamondlike carbon coating (~1500 kg/mm^2 as measured using a Berkovich indenter), and with or without top layer of perfluoropolyether lubricant coating. A (100) single-crystal silicon was also used for comparisons.

4.0 RESULTS AND DISCUSSION

4.1 Friction

Figures 4 to 7 are the surface profiles, the slopes of surface profiles taken along the sample sliding direction, and friction profiles for the tape and the unlubricated and textured disk for two scan sizes. No direct correlation between the surface profiles and the corresponding friction profiles is observed in these figures, e.g., high and low points on the friction profile do not correspond to high and low points on the roughness profile, respectively. However, there is a correlation between the slope of the roughness profiles and the corresponding friction profiles. In a paper by Bhushan and Ruan (**32**), we have presented evidence of similar correlation on a microscale of 500 nm x 500 nm for the tape and disk samples. We note that the AFM tip has a radius (typically about 30- to 50 nm) smaller than that of most asperities on the magnetic media [typically around 100-200 nm (**19**)], the slope of the sample surfaces taken in the sample sliding direction is expected to affect the local friction. According to the ratchet mechanism proposed by Makinson (**47**) [also see Bowden and Tabor (**48**)], the variation of friction is strongly correlated to the variation of the local surface slope, with the ascending edge of an asperity having a larger friction force than that at the descending edge.

Bhushan and Ruan (**32**) have previously measured macroscale friction of these magnetic media samples as those used in this study against a silicon nitride ball. We found that the macroscale coefficient of friction is about a factor of five larger than that of the average microscale coefficient of friction of the corresponding samples (**32**). Larger macro coefficient of friction may be the result of plowing effect associated with the macroscale measurement since visible wear scars were observed on the samples after the measurement. Bhushan and Ruan (**32**) had also observed the directionality in the local variation of micro-scale friction data as the samples were scanned in either direction, resulting from the scanning direction and the anisotropy in the surface topography.

4.2 Scratching and Wear

Tapes could be scratched at about 100 nN. With disks, surface deformation under a 100 nN normal load was not observable. It is possible that material removal did occur on an atomic scale which was not observable with a scan size of about 1 μm square. As the load is increased from nN range to μN range, severe scratches becomes visible for all samples tested. Figure 8 shows some of the scratching marks on a single-crystal (100) silicon, an unlubricated as-polished disk and a calendered metal-particle tape. All scratching were done with 10 cycles. Scratch depth as a function of load for the three samples is plotted in Fig. 9.

For silicon, gentle scratch marks were visible under a 10 μN load. At 40 μN load, the scratch mark is about 50 nm deep and the depth of scratch increases with load. For disks, on the other hand, a 40 μN load produced only a very gentle scratch (less than 10 nm). The scratch depth increased slightly at the load of 50 μN. Once the load is increased in excess of 60 μN, the scratch depth increased rapidly. We believe that the carbon coating on the disk surface is cracked at about 60 μN. This result indicates that the carbon coating is much harder to scratch than the underlying material (thin-film magnetic material) and silicon. This is expected since the diamondlike carbon coating is harder than silicon and the thin film magnetic material used in the construction of disk (**18**). For the tape sample, severe scratch is produced even at a low load of 4 μN.

By scanning the sample (in 2D) while scratching, wear scars were generated on the sample surface. Figure 10 shows the wear depth as a function of load for the as-polished, unlubricated and lubricated disks with one scratch cycle. Figure 11 shows profiles of the wear scars generated on an as-polished, unlubricated disk . The normal force for the imaging was about 0.5 μN and the loads used for the wear were 20, 50, 80 and 100 μN as indicated in the figure. We note that wear takes place relatively uniformly across the disk surface and appears to be essentially independent of the lubrication for the disks studied. For both lubricated and unlubricated disks, the wear depth increases slowly with load at low loads with almost the same wear rate. As the load is increased to about 60 μN, wear increases rapidly with load. The wear depth at 50 μN is about 14 nm, slightly less than the thickness of the carbon film. The rapid increase of wear with load at loads larger than 60 μN is an indication of the breakdown of the carbon coating on the disk surface.

Figure 12 shows the wear depth as a function of number of cycles for the as-polished disks (lubricated and unlubricated). Again, for both unlubricated and lubricated disks, wear initially takes place slowly with a sudden increase between 40 and 50 cycles at 10 μN. The sudden increase occurred after 10 cycles at 20 μN. This rapid increase is associated with the breakdown of the carbon coating. The wear profiles at various cycles are shown in Figs. 13 and 14 for an unlubricated as-polished disk at a normal load of 10 μN and 20 μN, respectively. At a load of 10 μN, wear takes place relatively uniformly across the disk surface, similar to those shown in Fig. 11. At a load of 20 μN (Fig. 14), wear is not uniform and the wear is largely initiated at the texture grooves present on the disk surface. This indicates that surface defects strongly affect the wear rate.

Corresponding wear results for the MP tape are shown in Figs. 15 to 18. The wear depth increases nearly linearly at low loads (<4 μN with 1 cycle) or with small number of cycles (<20 cycles at 2 μN). The increase of wear with load or with number of cycles becomes greater at a larger load (>5 μN, 1 cycle) or with a larger number of cycles (>25 at 2 μN).

4.3 Indentation

The mechanical properties of materials can also be measured using AFM. Figure 19(a) shows the gray scale plot of indentation marks generated with the diamond tip on a (111) silicon wafer at normal loads of 70 and 100 μN. The triangular shape of the indents is clearly observed. Figure 19(b) also shows the line plot of the inverted image of Fig. 19(a), indentation marks representing the shape of the diamond tip used in the indentation (Fig. 2). The residual areas of the indentation mark in Fig. 19 are about 4400 and 8600 nm^2 at 70 and 100 μN, from which the hardness values of silicon surface were calculated to be about 16 and 12 GPa, respectively. The hardness values for Si at 100 μN is comparable to the microhardness values for bulk Si reported by others (**49**).

As-polished disks were also indented at various loads. Figure 20 shows images of three indents made at a load of 80, 100, and 140 μN with calculated hardness values of 21 GPa, 21 GPa, and 9.0 GPa, respectively. The hardness value at 80 μN and 100 μN is much higher than at 140 μN. This is expected since the indentation depth is only about 10 nm at 80 μN and 15 nm at 100 μN which is smaller than the thickness of carbon coating (30 nm). The hardness value at lower loads is primarily the value of the carbon coating. The indentation depth at 140 μN is 40 nm. At this depth, the hardness value is primarily the value of the magnetic film, which is softer than the carbon coating (**18**). This result is consistent with the scratch and wear data discussed previously.

For the case of hardness measurements made on magnetic disks at low loads, indentation depth is on the same order as the variation in the surface roughness. For accurate measurements of indentation size and depth, it is desirable to subtract the original (unindented) profile from the indented profile. We developed an algorithm for this purpose. Because of PZT hysteresis, a translational shift in the sample plane occurs during the scanning period, resulting in a shift between images captured before and after indentation. Therefore, we need to shift the images for perfect overlap before subtraction can be performed. [A similar approach is also being pursued by Lu and Bogy (**50**).] To accomplish our objective, a small region on the original image was selected and attempt was made to find the corresponding region in the indented image by maximizing the correlation between the two regions. (Profiles were plane-fitted before subtraction.) Once the two regions were identified, overlapped areas between the two images were determined and the original image was shifted with the required translational shift and then subtracted from the indented image. An example of profiles before and after subtraction is shown in Fig. 21. It is easier to measure indent on the subtracted image.

4.4 Nanofabrication

A simple extension of nanoscratching is nanofabrication using AFM. Figure 22 shows such an example. The letters "CMCL" were written on a (100) single-crystal silicon using a diamond tip under a 40 μN normal force. The writing was done at a slow speed (0.2 μm/s for scratching each line). Some thermal drift of the PZT tube has occurred during the writing, resulting in small shift in the marks. With a totally automated operation, it is possible to significantly reduce the drifting effect and to improve the letter quality.

5.0 SUMMARY

It has been shown that atomic force microscopy and friction force microscopy can be used for various tribological studies. Data are presented which show that the ratchet mechanism is responsible for the variation of microscale friction for the disks and a tape studied. Diamondlike carbon coatings protects the disk surface up to a certain load. Once this carbon coating is broken, disk material wears out rapidly. Wear takes places much faster near texture grooves, indicating that surface defects strongly affect the wear properties of materials. Wear of tape surface is pretty linear with load. Nanoindentations were made on disks and on silicon and the hardnesses of the materials were calculated. Hardness at a penetration depth as low as 3 nm can be measured. AFM has also been shown to be useful for nanofabrication.

6.0 ACKNOWLEDGMENTS

The diamond tips used in this research were supplied by Dr. R. Kaneko of NTT Japan. This research was sponsored in part by the Office of the Chief of Naval Research (Department of the Navy), Advanced Research Projects Agency/National Storage Industry Consortium, and the Membership of the Computer Microtribology and Contamination Laboratory. The Contents of the information does not necessarily reflect the position or the policy of the Government and no official endorsement should be inferred.

References

1 **Binnig, G., Rohrer, H., Gerber, Ch. and Weibel, E.** Surface Studies by Scanning Tunneling Microscopy. Phys. Rev. Lett., 1982, **49(1),** 57-61.

2 **Melmed, A. J.** The Art and Science and Other Aspects of Making Sharp Tips. J. Vac. Sci. Technol. B, 1991 **9(2)**, 601-608.

3 **Binnig, G., Quate, C. F. and Gerber, Ch.** Atomic Force Microscope. Phys. Rev. Lett., 1986, **56(9)**, 930-933.

4 **Israelachvili, J. N. and Adams, G. E.** Measurement of Friction between Two Mica Surfaces in Aqueous Electrolyte Solutions in the Range 0-100 nm. Chem. Soc. J., Faraday Trans. I, 1978, **74**, 975-1001.

5 **Israelachvili, J. N., McGuiggan, P. M., and Homola, A. M.** Dynamic Properties of Molecularly Thin Liquid Films. Science, 1988, **240**, 189-190.

6 **Van Alsten, J., and Granick, S.** Molecular Tribology of Ultrathin Liquid Films. Phys. Rev. Lett., 1988, **61(22)**, 2570-2573.

7 **Granick, S.** Motions and Relaxations of Confined Liquids. Science, 1991, **253**, 1374-1379.

8 **Albrecht, T. R., Akamine, S., Carver, T. E., and Quate, C. F.,** Microfabrication of Cantilever Styli for the Atomic Force Microscope. J. Vac. Sci and Technol. A, 1990, **8(4)**, 3386-3396.

9 **McClelland, G. M., Erlandsson, R., and Chiang, S.** Atomic Force Microscopy: General Principles and a New Implementation. In Review of Progress in Quantitative Nondestructive Evaluation, 1987 (D. O. Thompson and D. E. Chimenti, eds.), **6B**, 1307-1314 (Plenum, NY).

10 **Mate, C. M., McClelland, G. M., Erlandsson, R., and Chiang, S.** Atomic-Scale Friction of a Tungsten Tip on a Graphite Surface. Phys. Rev. Lett., 1987, **59(17)**, 1942-1945.

11 **Erlandsson, R., McClelland, G. M., Mate, C. M. and Chiang, S.** Atomic Force Microscopy Using Optical Interferometry. J. Vac. Sci. Technol. A, 1988, **6(2)**, 266-270.

12 **Martin, Y., Williams, C. C., and Wickramasinghe, H. K.** Atomic Force Microscope-Force Mapping and Profiling on a Sub 100-Å Scale. J. Appl. Phys., 1987, **61(10)**, 4723-4729.

13 **Albrecht, T. R. and Quate, C. F.** Atomic Resolution Imaging of a Nonconductor by Atomic Force Microscopy. J. Appl. Phys., 1987, **62(7)**, 2599-2602.

14 **Marti, O., Drake, B. and Hansma, P. K.** Atomic Force Microscopy of Liquid-Covered Surfaces: Atomic Resolution Images. Appl. Phys. Lett., 1987, **51(7)**, 484-486.

15 **Meyer, G. and Amer, N. M.** Optical-Beam-Deflection Atomic Force Microscopy: The NaCl (001) Surface. Appl. Phys. Lett., 1990, **56(21)**, 2100-2101.

16 **Maivald, P., Butt, H. J., Gould, S. A. C., Prater, C. B., Drake, B., Gurley, J. A., Elings, V. B. and Hansma, P. K.** Using Force Modulation to Image Surace Elasticities with the Atomic Force Microscope. Nanotechnology, 1991, **2(2)**, 103-106.

17 **Radmacher, M., Tillman, R. W., Fritz-Stephan, M. and Gaub, H. E.** From Molecules to Cells - Imaging Soft Samples with the Soft Samples. Science, 1993 (in press).

18 **Bhushan, B.** Tribology and Mechanics of Magnetic Storage Devices, 1990 (Springer Verlag, New York).

19 **Bhushan, B. and Blackman, G. S.** Atomic Force Microscopy of Magnetic Rigid Disks and Sliders and Its Applications to Tribology. J. Trib., Trans. ASME, 1991, **113**, 452-458.

20 **Oden, P. I., Majumdar, A., Bhushan, B., Padmanabhan, A. and Graham, J. J.** AFM Imaging, Roughness Analysis and Contact Mechanics of Magnetic Tape and Head Surfaces. J. Trib., Trans. ASME, 1992, **114**, 666-674.

21 **Kaneko, R. and Enomoto, Y.** (eds.) Proc. 1st Int. Workshop on Microtribology, 1992, (The Jap. Soc. of Tribologists, Tokyo, Japan, October).

22 **Martin, Y., Wickramasinghe, H. K.** Magnetic Imaging by Force Microscopy with 1000 Å Resolution. Appl. Phys. Lett., 1987, **50(20)**, 1455-1457.

23 **Schonenberger, C. and Alvarado, S. F.** Understanding Magnetic Force Microscopy. Z. Phys. B. (Germany), 1990, **80(3)**, 373-383.

24 **Grütter, P., Ruger, D., Mamin, H.J., Castillo, G., Lin, C.-J., McFadyen, I. R., Valletta, R. M., Wolter, O., Bayer, T., and Greschner, J.** Magnetic Force Microscopy with Batch-Fabricated Force Sensors. J. Appl. Phys., 1991, **69(8)**, 5883-5885.

25 **Manne, S., Hansma, P.K., Massie, J., Elings, V. B. and Gewirth, A. A.** Atomic-Resolution Electrochemistry with the Atomic Force Microscope: Copper Depoition on Gold. Science, 1991, **251**, 183-186.

26 **Hoh, J. H., Cleveland, J. P., Prater, C. B., Revel, J. P. and Hansma, P. K.** Quantized Adhesion Detected with the Atomic Force Microscope. J. Amer. Chem. Soc., 1992, **114**, 4917-4918.

27 **Hues, S. M., Colton, R.J., Meyer, E. and Guntherodt, H-J,** Scanning Probe Microscopy of Thin Film. MRS Bulletin, 1993, **Jan.**, 41-49.

28 **Weisenhorn, A. L., Maivald, P., Butt, H. J., and Hansma, P. K.** Measuring Adhesion, Attraction, and Repulsion Between Surfaces in Liquids with an Atomic-Force Microscope. Phys. Rev. B, 1992, **45(19)**, 11226-11232.

29 **Kaneko, R., Miyamoto, T. and Hamada, E.** Development of a Controlled Friction Force Microscope and Imaging of Recording Disk Surfaces. Adv. Inf. Storage Syst., 1991, **1**, 267-277.

30 **Meyer, G. and Amer, N. M.** Simultaneous Measurement of Lateral and Normal Forces with an Optical-Beam-Deflection Atomic Force Microscope. Appl. Phys. Lett., 1990, **57(20)**, 2089-2091.

31 **Ruan, J. and Bhushan, B.** Atomic-Scale Friction Measurements Using Friction Force Microscopy Part I - General Principles and New Measurement Techniques. J. Trib., Trans. ASME, 1994 (in press).

32 **Bhushan, B. and Ruan, J.** Atomic-Scale Friction Measurements Using Friction Force Microscopy Part II - Application to Magnetic Media. J. Trib., Trans. ASME, 1994 (in press).

33 **Ruan, J. and Bhushan, B.** Nanoindentation Studies of Fullerene Films Using Atomic Force Microscopy. J. Mat. Res., 1993 (in press).

34 **Mate, C. M., Lorenz, M. R., and Novotny, V. J.** Atomic Force Microscopy of Polymeric Liquid Films. J. Chem. Phys., 1989, **90(12)**, 7550-7555.

35 **Blackman, G. S., Mate, C. M. and Philpott, M. R.** Interaction Forces of a Sharp Tungsten tip with Molecular Films on Silicon Surface. Phys. Rev. Lett., 1990, **65(18)**, 2270-2273.

36 **Frommer, J.** Scanning Tunneling Microscopy and Atomic Force Microscopy in Organic Chemistry. Angew. Chem. Int. Ed. Engl., 1992, **31**, 1298-1328.

37 **Meyer, E., Overney, R., Lüthi, R., Brodbeck, D., Howald, L., Frommer, J., Güntherodt, H.-J, Wolter, O., Fujihira, M., Takano, T., and Gotoh, Y.** Friction

Force Microscopy of Mixed Langmuir-Blodgett Films. Thin Solid Films, 1992, **220**, 132-137.

38 **Overney, R. M., Meyer, E., Frommer, J., Brodbeck, D., Lüthi, R., Howard, L., Güntherodt, H.-J., Fujihira, M., Takano, H., and Gotoh, Y.** Friction Measurements on Phase-Separated Thin Films with a Modified Atomic Force Microscope. Nature, 1992, **359**, 133-135.

39 **O'Shea, S. J. and Welland, M. E.** Atomic Force Microscope Study of Boundary Layer Lubrication. Appl. Phys. Lett., 1992, **61(18)**, 2240-2242.

40 **Ohkubo, T., Kishigami, J., Yanagisawa, K., and Kaneko, R.** Submicron Magnetizing and Its Detection Based on the Point Magnetic Recording Concept. IEEE Trans. Magn., 1991, **27(6)**, 5286-5288.

41 **Andoh, Y., Oguchi, S., Kaneko, R. and Miyamoto, T.** Evaluation of Very Thin Lubricant Films. J. Phys. D: Appl. Phys., 1992, **25**, A71-A75.

42 **Majumdar, A., Carrejo, J. P., and Lai, J.** Thermal Imaging Using the Atomic Force Microscope. Appl. Phys. Lett., 1993, **62(20)**, 2501-2503.

43 **Burnham, N. A. and Colton, R. J.** Measuring the Nanomechanical Properties and Surface Forces of Materials Using an Atomic Force Microscope. J. Vac. Sci. Technol. A, 1989, **7(4)**, 2906-2913.

44 **Majumdar, A., Oden, P. I., Carrejo, J. P., Nagahara, L. A., Graham, J. J. and Alexandar, J.** Nanometer-Scale Lithography Using the Atomic Force Microscope. Appl. Phys. Lett., 1992, **61(19)**, 2293-2295.

45 **Kobayashi, A., Grey, F., Williams, R. S. and Ano, M.** Formation of Nanometer-Scale Grooves in Silicon with a Scanning Tunneling Microscope. Science, 1993, **259**, 1724-1726.

46 **Alexander, S., Hellemans, L., Marti, O., Schneir, J., Elings, V., and Hansma, P. K.** An Atomic-Resolution Atomic-Force Microscope Implemented Using an Optical Lever. J. Appl. Phys., 1989, **65 (1)**, 164-167.

47 **Makinson, K. R.** On the Cause of the Frictional Difference of the Wool Fiber. Trans. Faraday Soc., 1948, **44**, 279-282.

48 **Bowden, F. P. and Tabor, D.** The Friction and Lubrication of Solids, 1950, 172-175 (Clarendon Press, Oxford).

49 **Pharr, G. M., Oliver, W. C., and Clarke, D. R.** The Mechanical Behavior of Silicon During Small-Scale Indentation. J. Electronic Materials, 1990, **19 (9)**, 881-887.

50 **Lu, C. J. , and Bogy, D. B.** personal communication, 1993.

Figure Captions

1. Schematic of AFM/FFM instrument.

2. (a) Schematics and (b) SEM micrographs of a PECVD Si_3N_4 cantilever beam with tip and a stainless steel cantilever beam with diamond tip.

3. Schematic of AFM tip trajectory on sample surfaces as the sample is scanned in two dimensions. Scratch and wear take place along both the solid and dotted lines whereas during imaging, data are recorded only during scans along the solid lines.

4. A 200 nm x 200 nm scan of a calendered metal-particle tape. (a) Surface roughness profile (σ= 6.1 nm), (b) slope of the roughness profile taken in the sample sliding direction (the horizontal axis) (mean=-0.04, σ=0.30), and (c) friction profile (mean=5.7 nN, σ=2.2 nN) for a normal load of 80 nN. (σ is the standard deviation.)

5. A 40 nm x 40 nm scan of a calendered metal-particle tape (a) Surface roughness profile (σ=2.8 nm), (b) slope of the roughness profile (mean=0.12, σ=0.45), and (c) friction profile (mean=5.1 nN, σ=3.1 nN) for a normal load of 80 nN.

6. A 200 nm x 200 nm scan of an unlubricated, textured disk. (a) Surface roughness profile (σ=2.9 nm), (b) slope of the roughness profile (mean=-0.03, σ=0.22), and (c) friction profile (mean=5.7 nN, σ=1.6 nN) for a normal load of 140 nN.

7. A 40 nm x 40 nm scan of an unlubricated textured disk. (a) Surface roughness profile (σ=1.2 nm), (b) slope of the roughness profile (mean=-0.08, σ=1.05), and (c) friction profile (mean=4.9 nN, σ=2.4 nN) for a normal load of 140 nN.

8. Surface profile for scratched (a) (100) single-crystal silicon, (b) unlubricated as-polished disk, and (c) MP tape. Samples were scratched for 10 cycles. The load used for various scratches are indicated in the plot.

9. Scratch depth as a function of load for (100) single-crystal silicon, an unlubricated as-polished disk and a MP tape shown in Fig. 8.

10. Wear depth as a function of load for both lubricated and unlubricated as-polished disks after one cycle.

11. Surface profile of an as-polished unlubricated disk showing the worn region (center 2μm x 2 μm) after one cycle of wear. The normal load and the number of test cycles are indicated in the figure.

12. Wear depth as a function of number of cycles for as-polished, lubricated and unlubricated disks at 10 μN and for an as-polished, unlubricated disk at 20 μN.

13. Surface profile of an as-polished unlubricated disk showing the worn region (center 2μm x 2 μm). The normal load and the number of test cycles are indicated in the figure.

14. Surface profile of an as-polished, unlubricated disk showing the worn region (center 2μm x 2 μm). The normal load and the number of test cycles are indicated in the figure.

15. Wear depth as a function of load for a calendered MP tape after one cycle.

16. Surface profile of a calendered MP tape showing the worn region (center 2μm x 2 μm). The normal load and the number of test cycles are indicated in the figure.

17. Wear depth as a function of number of cycles for a calendered MP tape at 2 μN.

18. Surface profile of a calendered MP tape worn (center 2μm x 2 μm region). The normal load and the number of test cycles are indicated in the figure.

19. (a) Gray scale plot and (b) inverted line plot of indentation marks on (111) single-crystal silicon at 70 and 100 μN.

20. Nanoindentation marks generated on an unlubricated as-polished disk. The normal load used in the indentation, the indentation depths and the hardness values are indicated in the figure.

21. Images with nanoindentation marks generated on an unlubricated as-polished disk at 140 μN (a) before subtraction, and (b) after subtraction.

22. Example of nanofabrication. The letters "CMCL" (which stands for Computer Microtribology and Contamination Laboratory) were generated by scratching a (100) silicon surface using a diamond tip at a normal load of 40 μN.

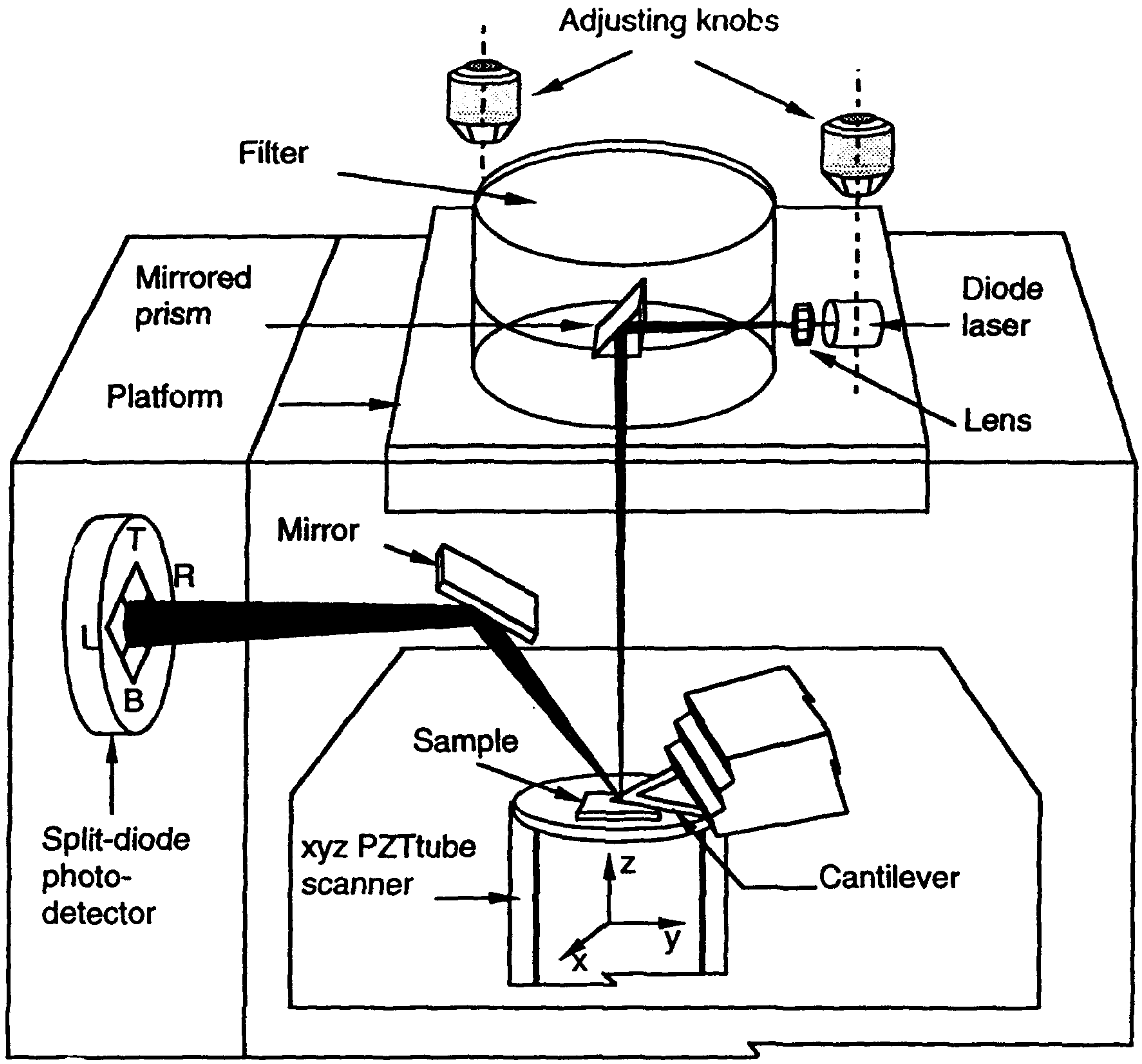

Adjusting knobs
Filter
Mirrored prism
Diode laser
Platform
Lens
Mirror
T
R
L
B
Sample
Split-diode photo-detector
xyz PZTtube scanner
z
y
x
Cantilever

Fig. 1

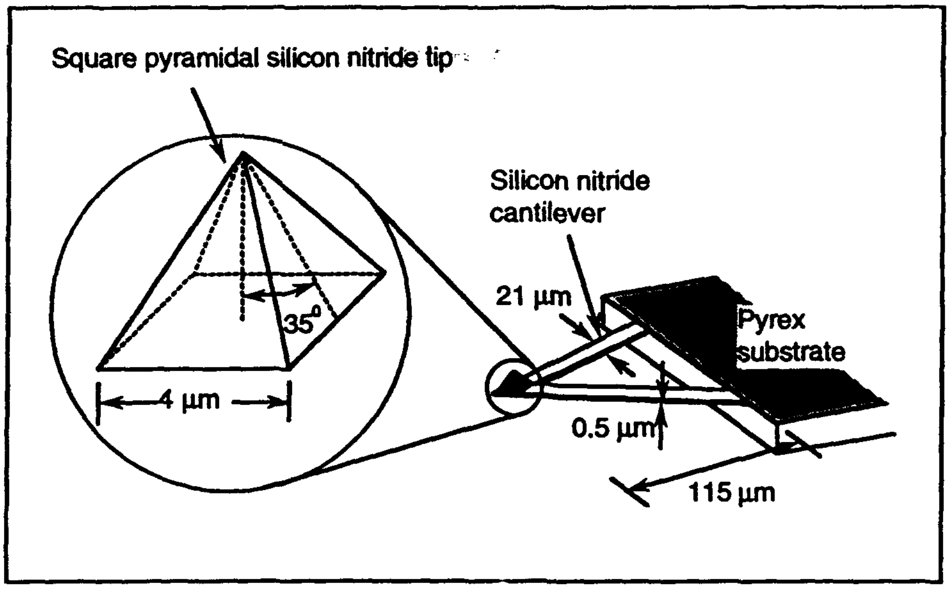

Square pyramidal silicon nitride tip
35°
4 μm
Silicon nitride
cantilever
21 μm
Pyrex
substrate
0.5 μm
115 μm

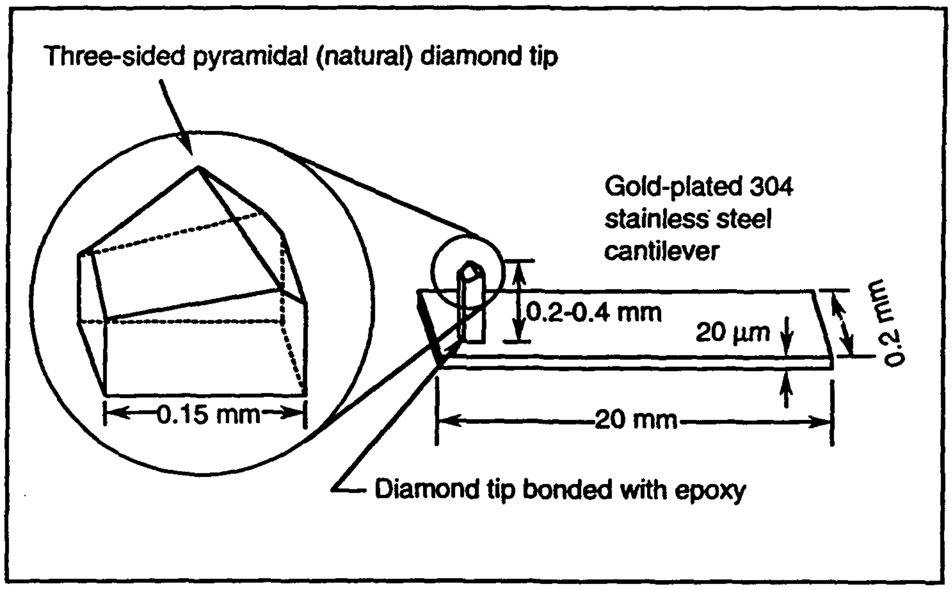

Three-sided pyramidal (natural) diamond tip
Gold-plated 304
stainless steel
cantilever
0.2-0.4 mm
20 μm
0.2 mm
0.15 mm
20 mm
Diamond tip bonded with epoxy

Fig. 2a

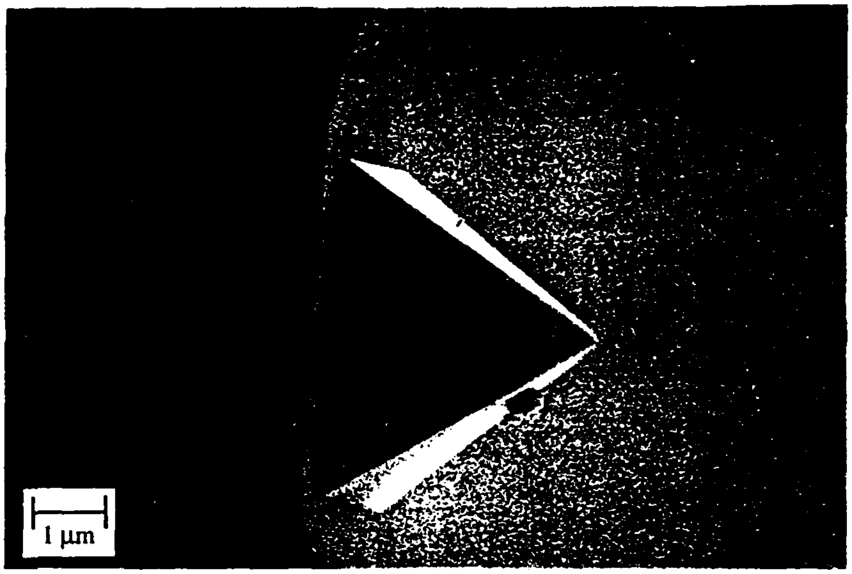

Square pyramidal silicon nitride tip

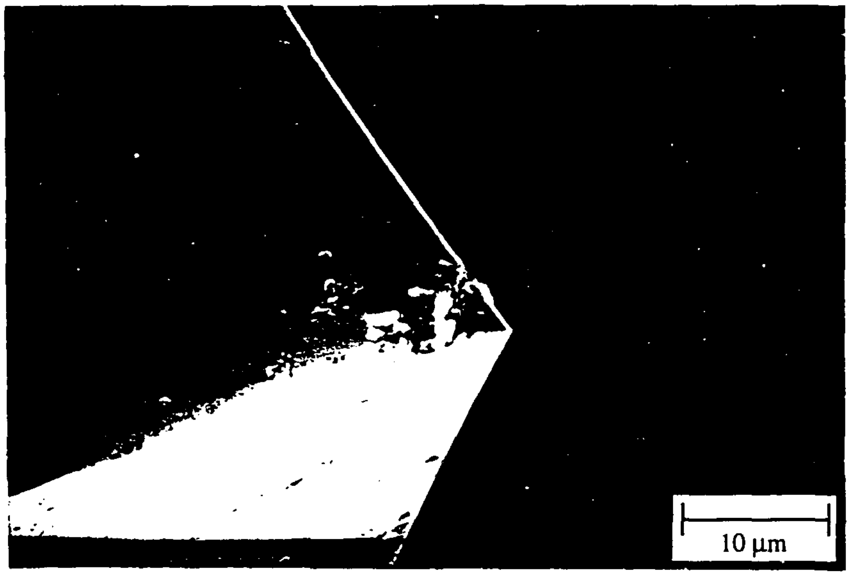

Three-sided pyramidal (natural) diamond tip

Fig. 2b

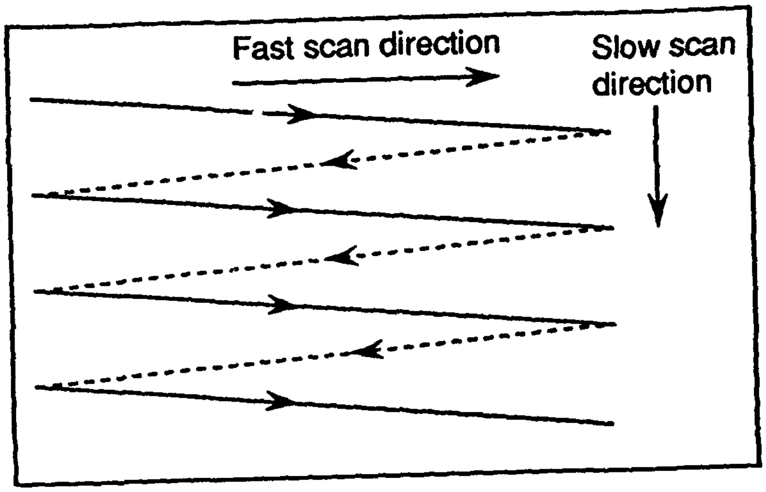

Fig. 3

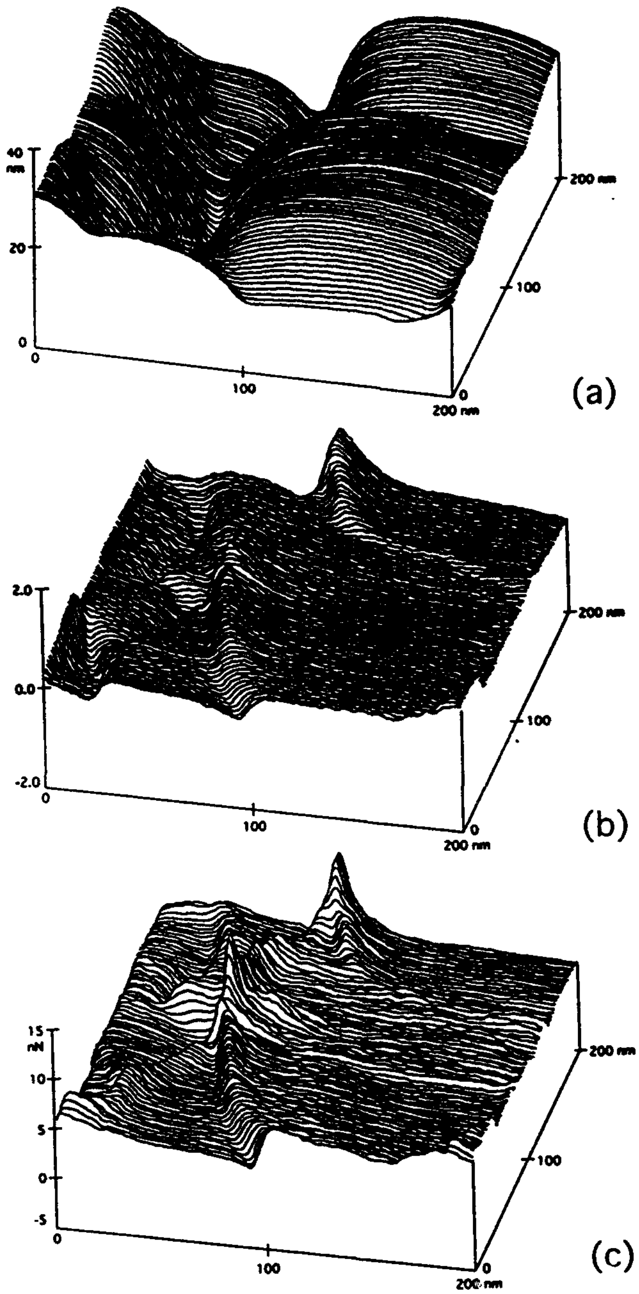
40
nm
20
0
0
100
200 nm
0
200 nm
100
200 nm
(a)
2.0
0.0
-2.0
0
100
200 nm
0
100
200 nm
(b)
15
nN
10
5
0
-5
0
100
200 nm
0
100
200 nm
(c)

Fig. 4

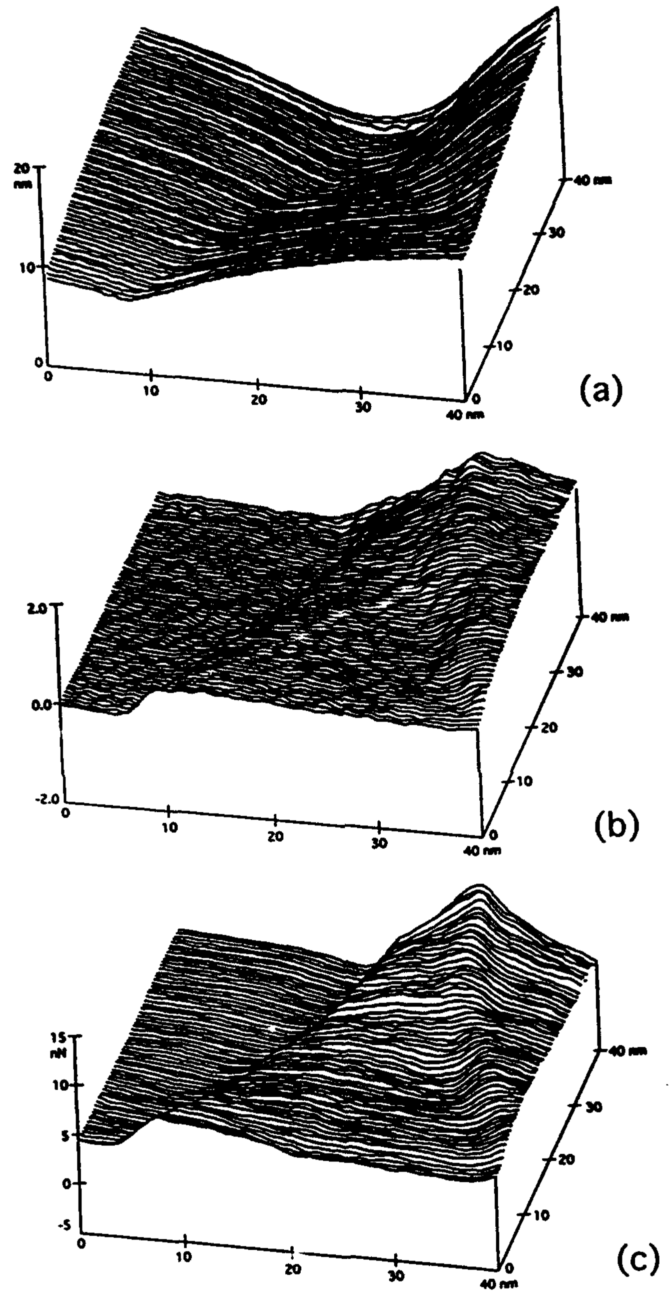

20 nm
10
0
0
10
20
30
40 nm
0
10
20
30
40 nm
(a)
2.0
0.0
-2.0
0
10
20
30
40 nm
0
10
20
30
40 nm
(b)
15 nN
10
5
0
-5
0
10
20
30
40 nm
0
10
20
30
40 nm
(c)

Fig. 5

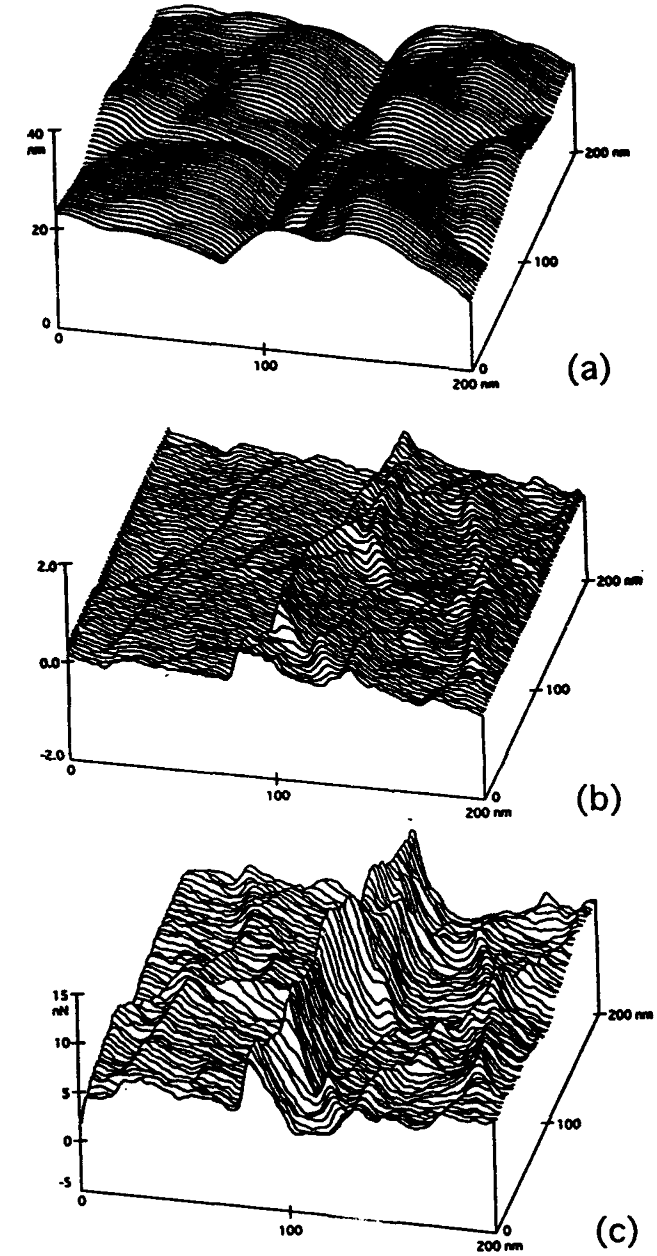
40 nm
20
0
0
100
200 nm
100
200 nm
(a)
2.0
0.0
-2.0
0
100
200 nm
100
200 nm
(b)
15 nN
10
5
0
-5
0
100
200 nm
100
200 nm
(c)

Fig. 6

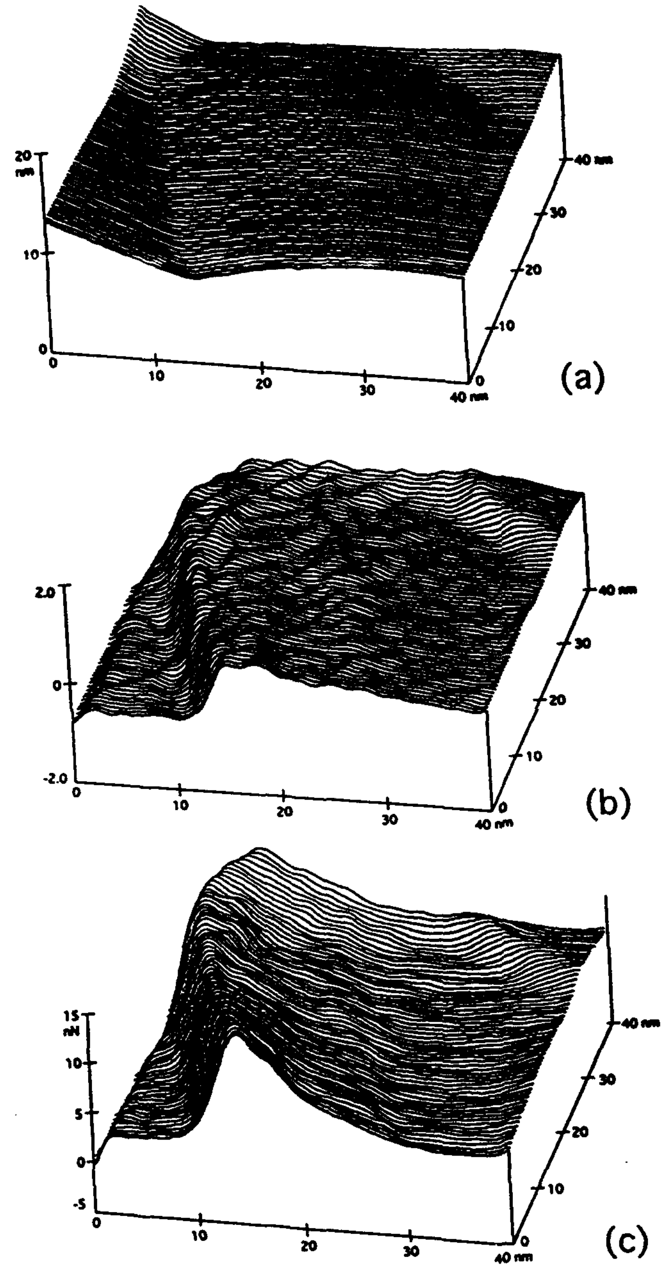

Fig. 7

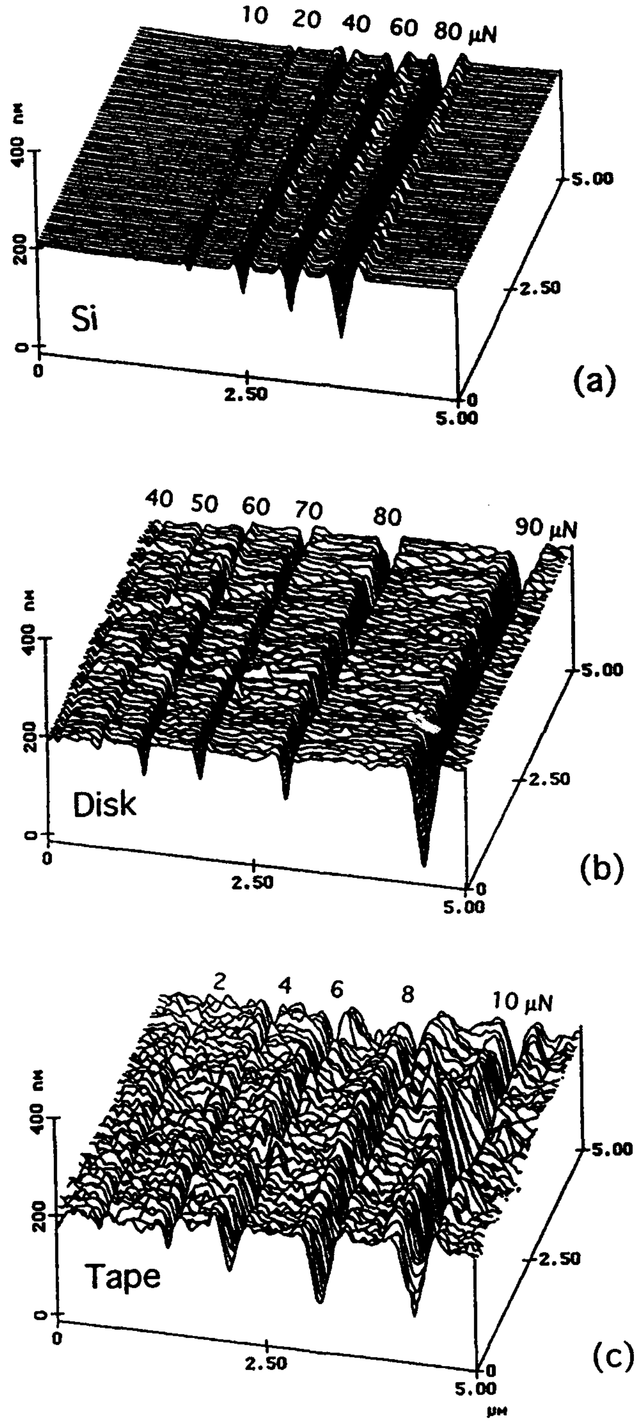

Fig. 8

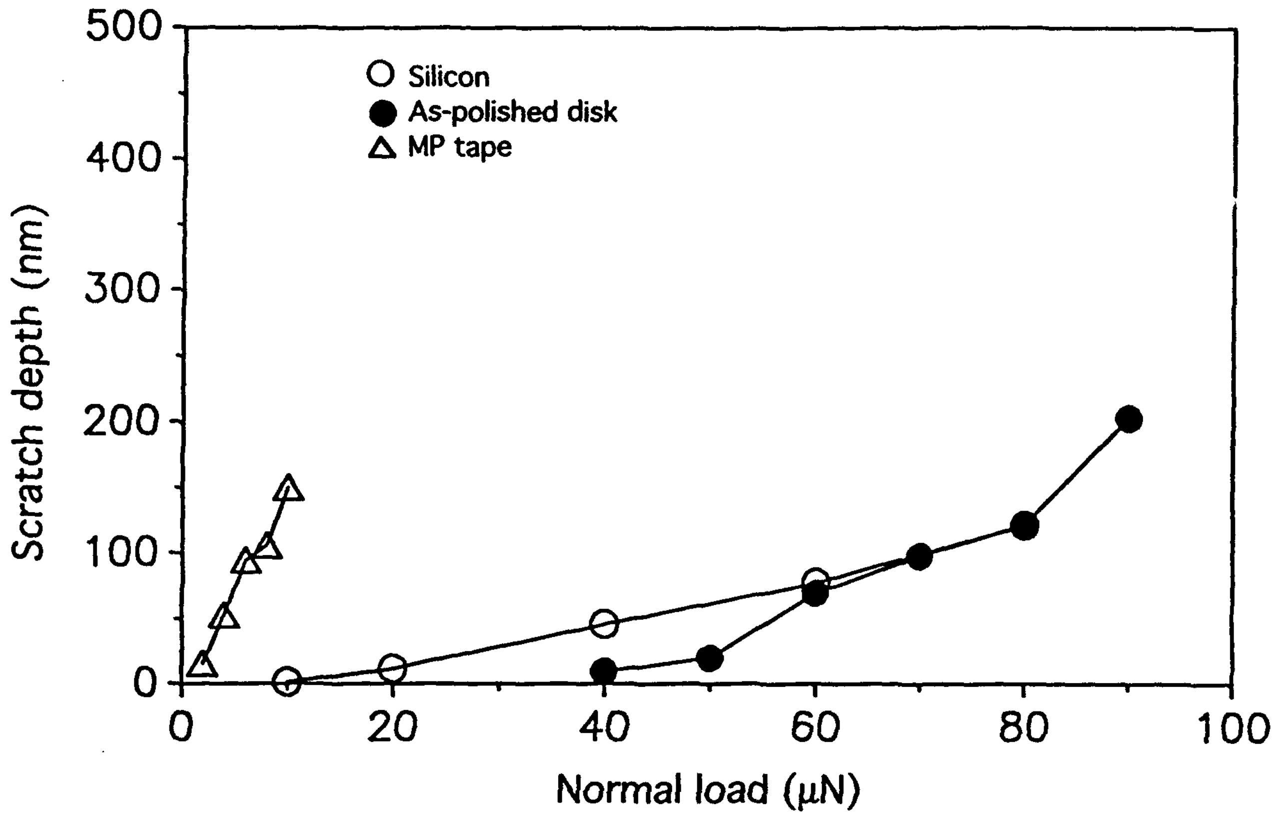

500
400
300
200
100
0
Scratch depth (nm)
0
20
40
60
80
100
Normal load (μN)
Silicon
As-polished disk
MP tape

Fig. 9

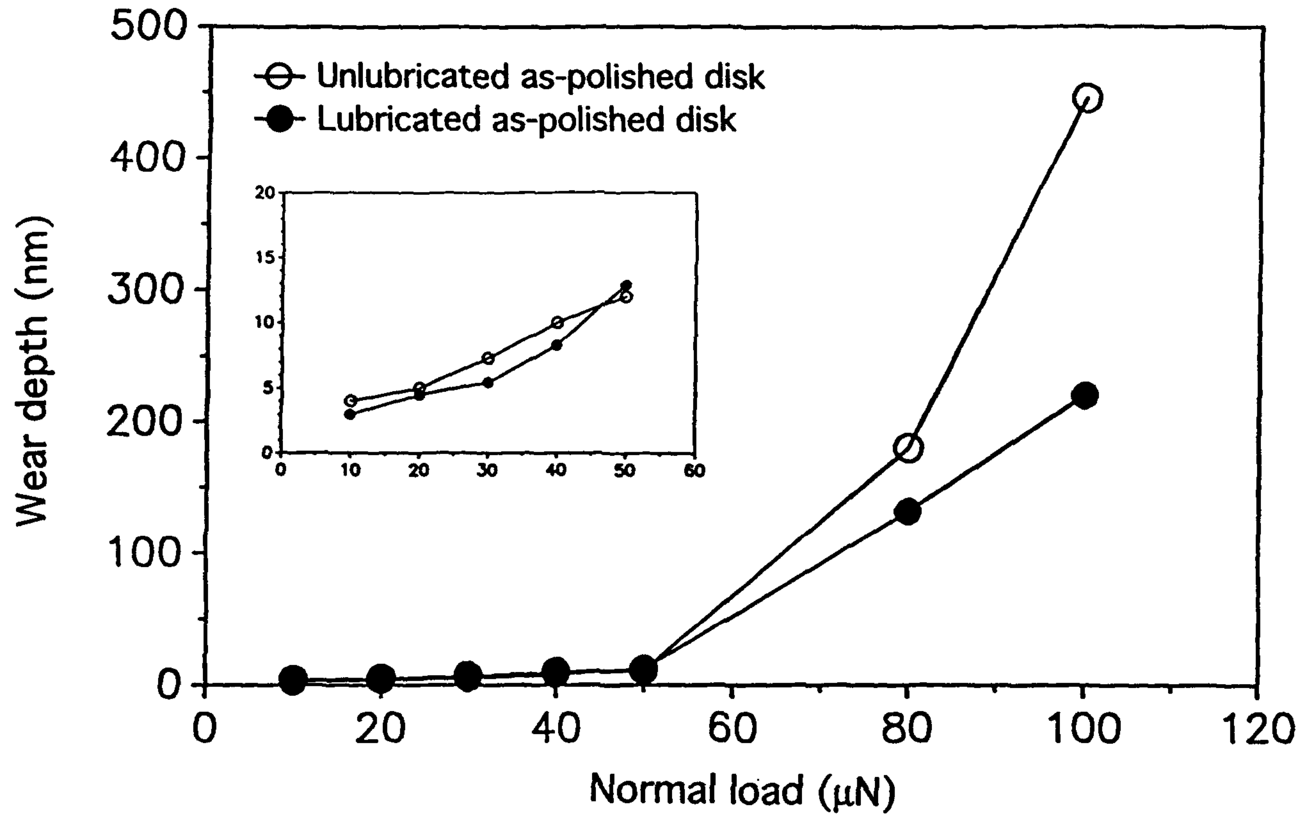

Unlubricated as-polished disk
Lubricated as-polished disk
Wear depth (nm)
Normal load (μN)
0
100
200
300
400
500
0
20
40
60
80
100
120
0
5
10
15
20
0
10
20
30
40
50
60

Fig. 10

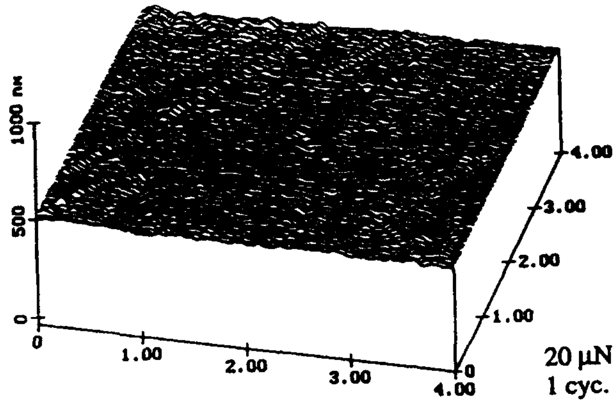
1000 nm
500
0
0
1.00
2.00
3.00
4.00
1.00
2.00
3.00
4.00
0
20 µN
1 cyc.

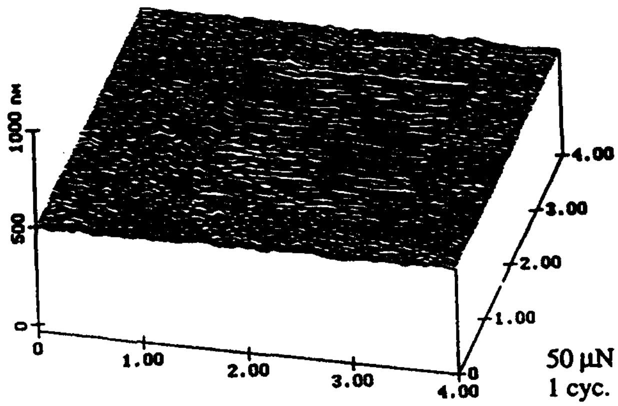
1000 nm
500
0
0
1.00
2.00
3.00
4.00
1.00
2.00
3.00
4.00
0
50 µN
1 cyc.

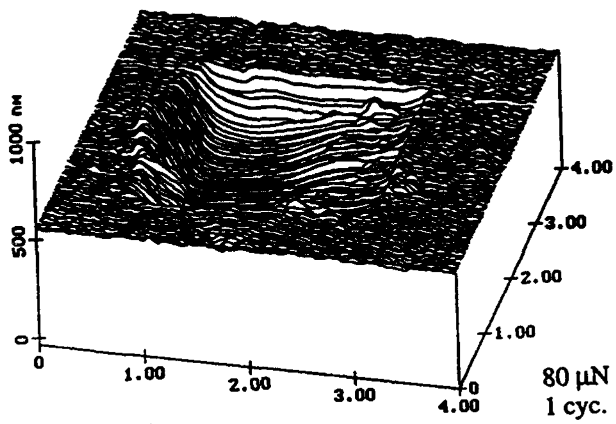
1000 nm
500
0
0
1.00
2.00
3.00
4.00
1.00
2.00
3.00
4.00
0
80 µN
1 cyc.

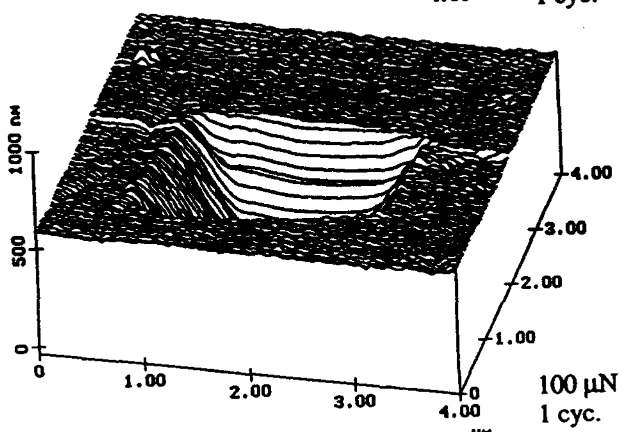
1000 nm
500
0
0
1.00
2.00
3.00
4.00
µm
1.00
2.00
3.00
4.00
0
100 µN
1 cyc.

Fig. 11

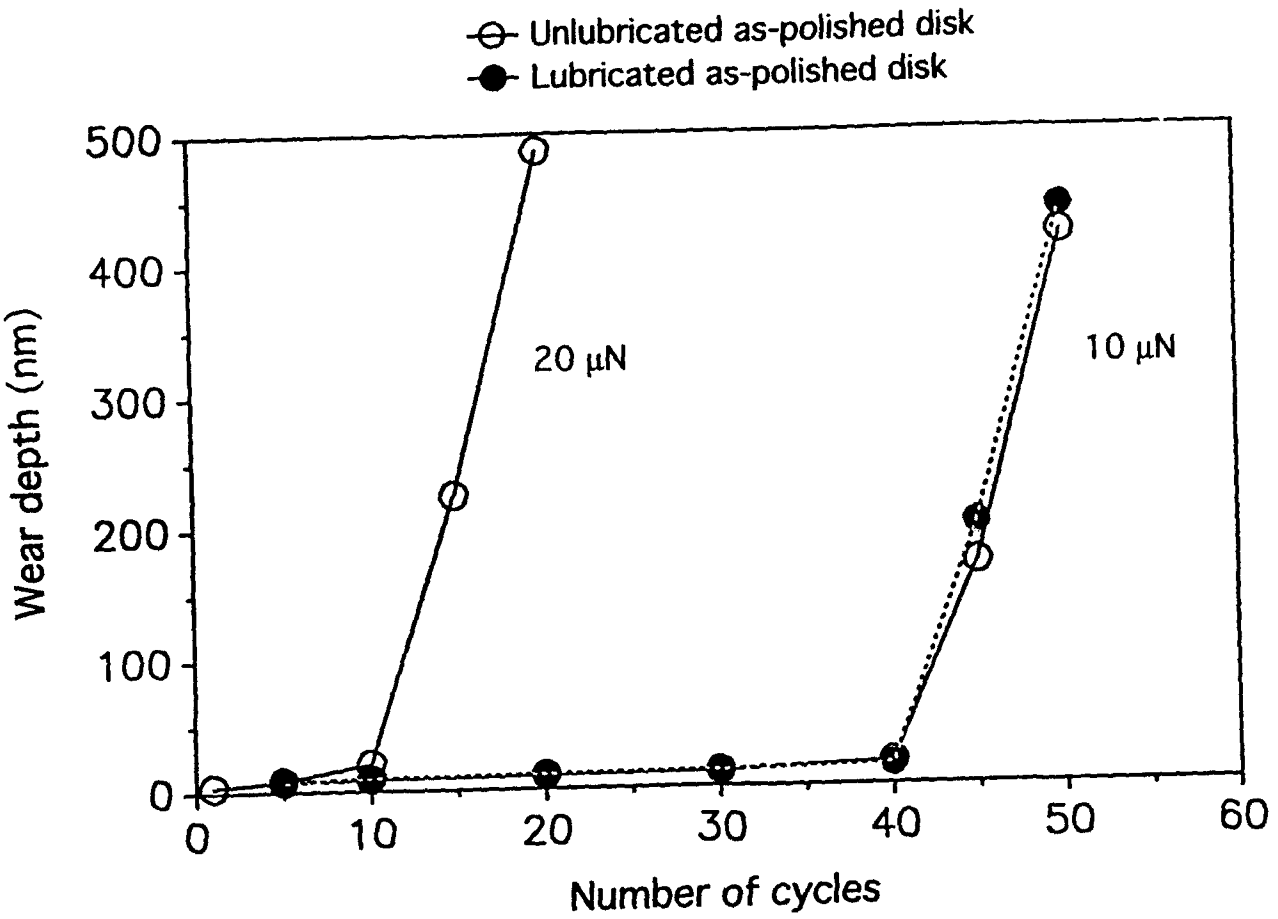

Unlubricated as-polished disk
Lubricated as-polished disk
Wear depth (nm)
500
400
300
200
100
0
20 µN
10 µN
0
10
20
30
40
50
60
Number of cycles

Fig. 12

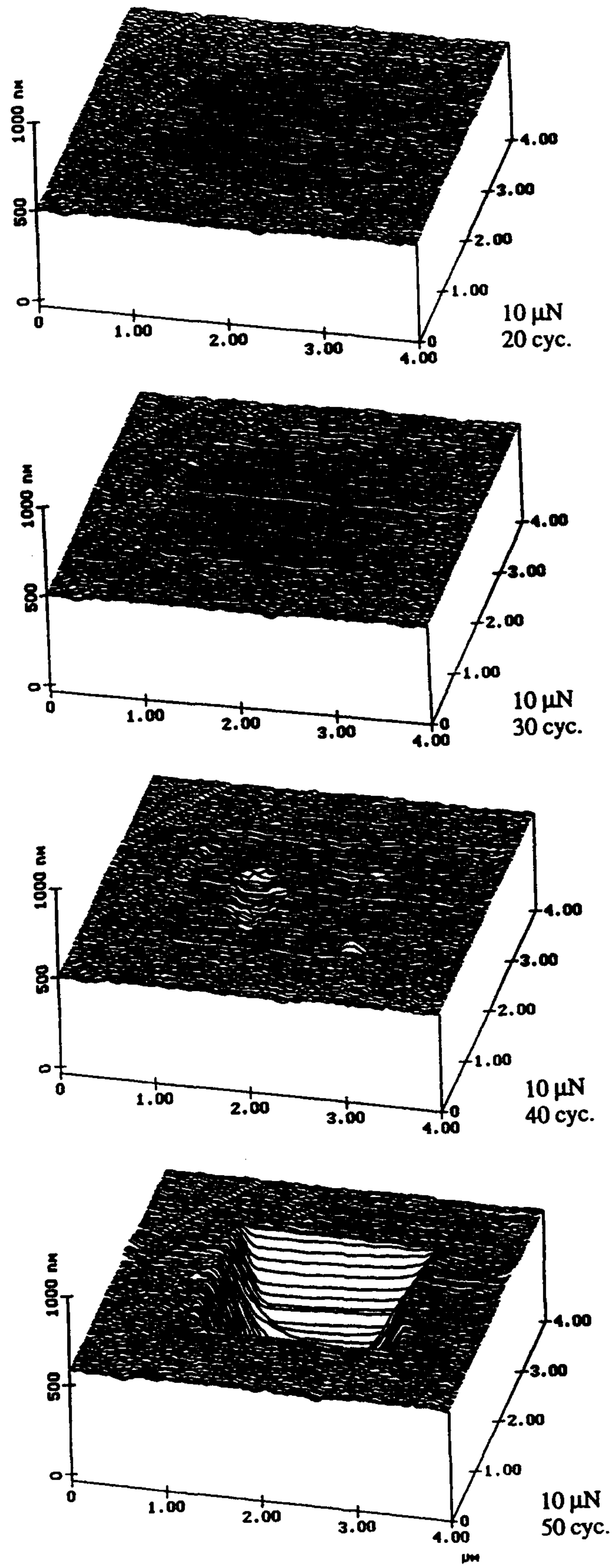
1000 nM
500
0
0
1.00
2.00
3.00
4.00
1.00
2.00
3.00
4.00
10 µN
20 cyc.
1000 nM
500
0
0
1.00
2.00
3.00
4.00
1.00
2.00
3.00
4.00
10 µN
30 cyc.
1000 nM
500
0
0
1.00
2.00
3.00
4.00
1.00
2.00
3.00
4.00
10 µN
40 cyc.
1000 nM
500
0
0
1.00
2.00
3.00
4.00
µM
1.00
2.00
3.00
4.00
10 µN
50 cyc.

Fig. 1

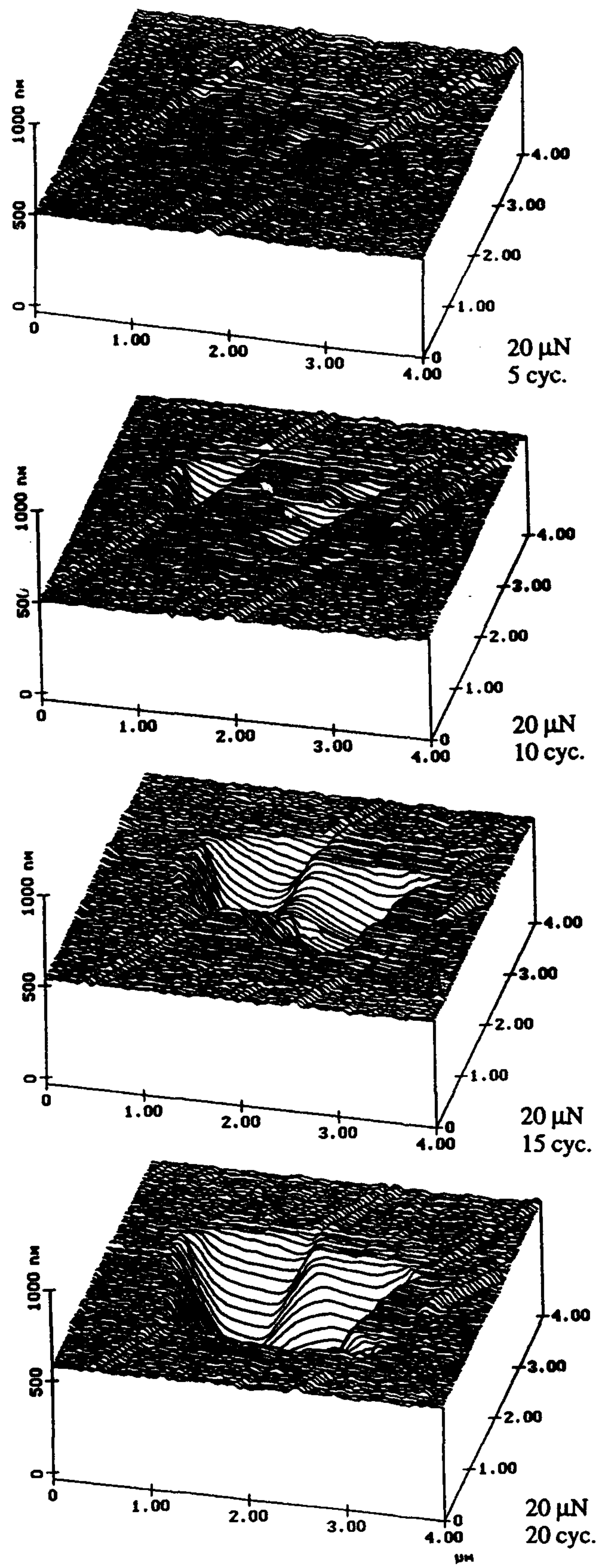
1000 nm
500
0
1.00
2.00
3.00
4.00
µm
20 µN
5 cyc.
20 µN
10 cyc.
20 µN
15 cyc.
20 µN
20 cyc.

Fig. 14

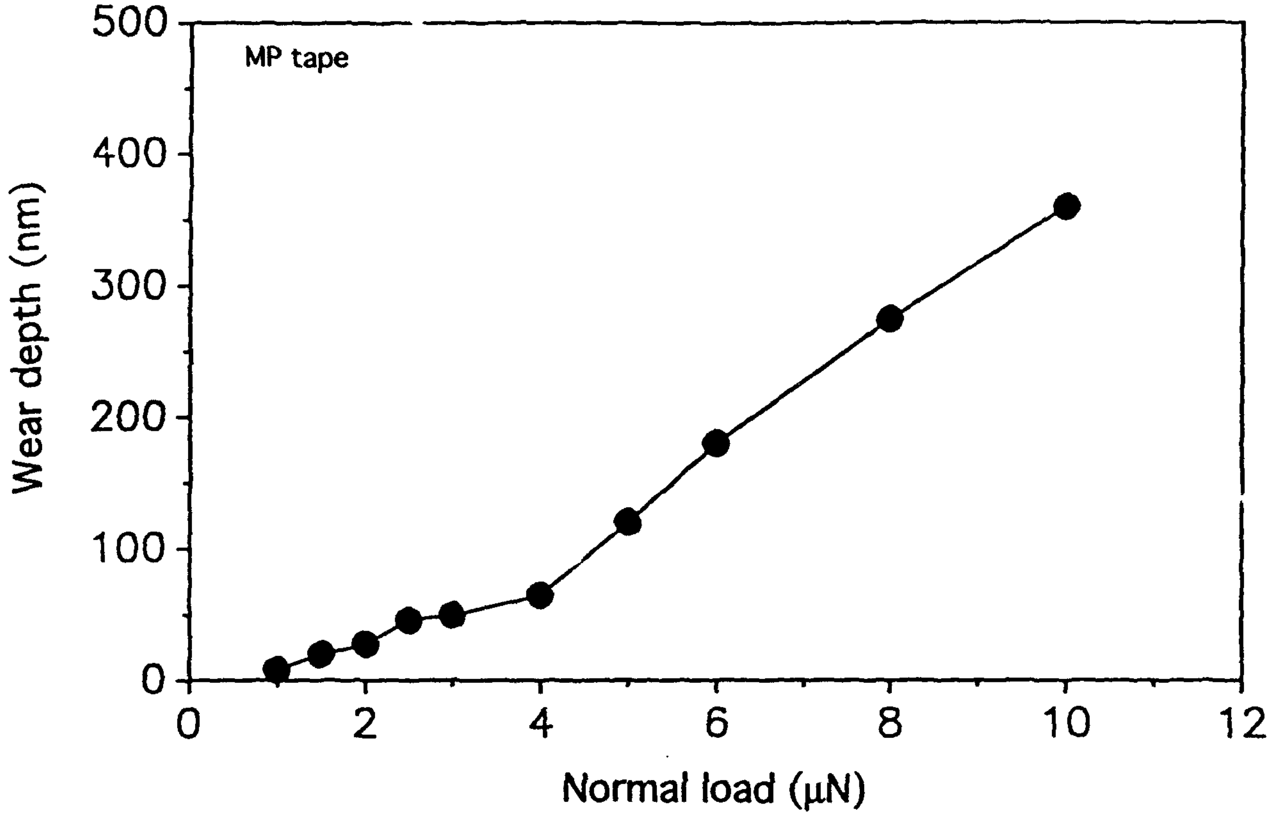
MP tape
Wear depth (nm)
Normal load (μN)
0
100
200
300
400
500
0
2
4
6
8
10
12

Fig. 15

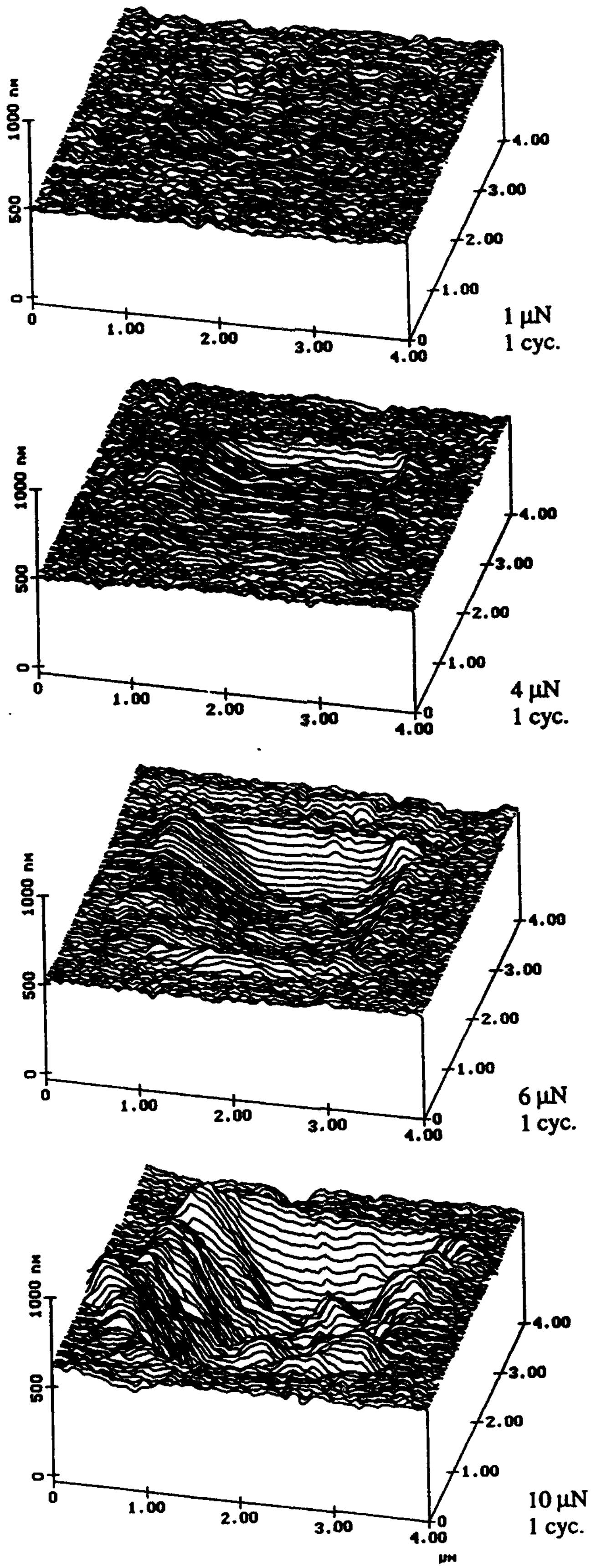
1000 nm
500
0
1.00
2.00
3.00
4.00
1 µN
1 cyc.
4 µN
1 cyc.
6 µN
1 cyc.
10 µN
1 cyc.
µm

Fig. 16

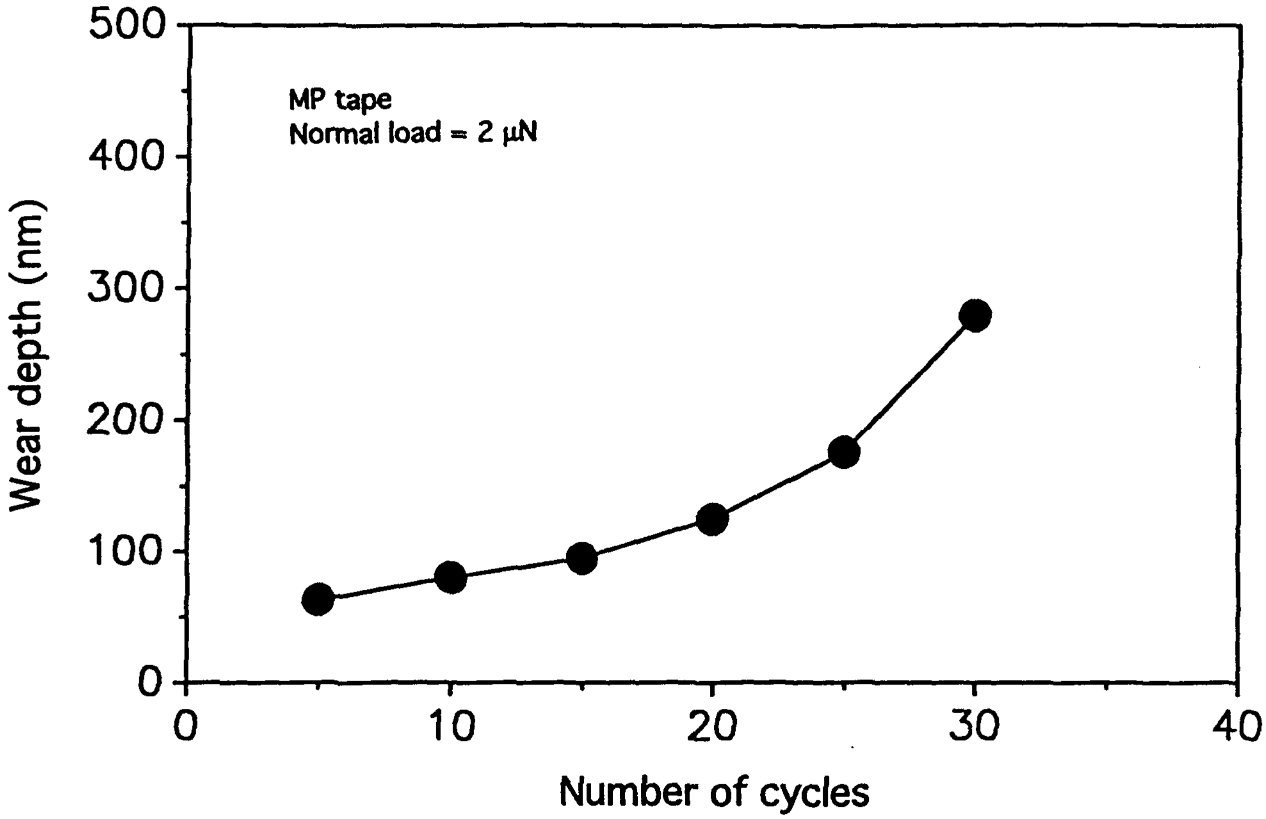
MP tape
Normal load = 2 μN
Wear depth (nm)
500
400
300
200
100
0
0
10
20
30
40
Number of cycles

Fig. 17

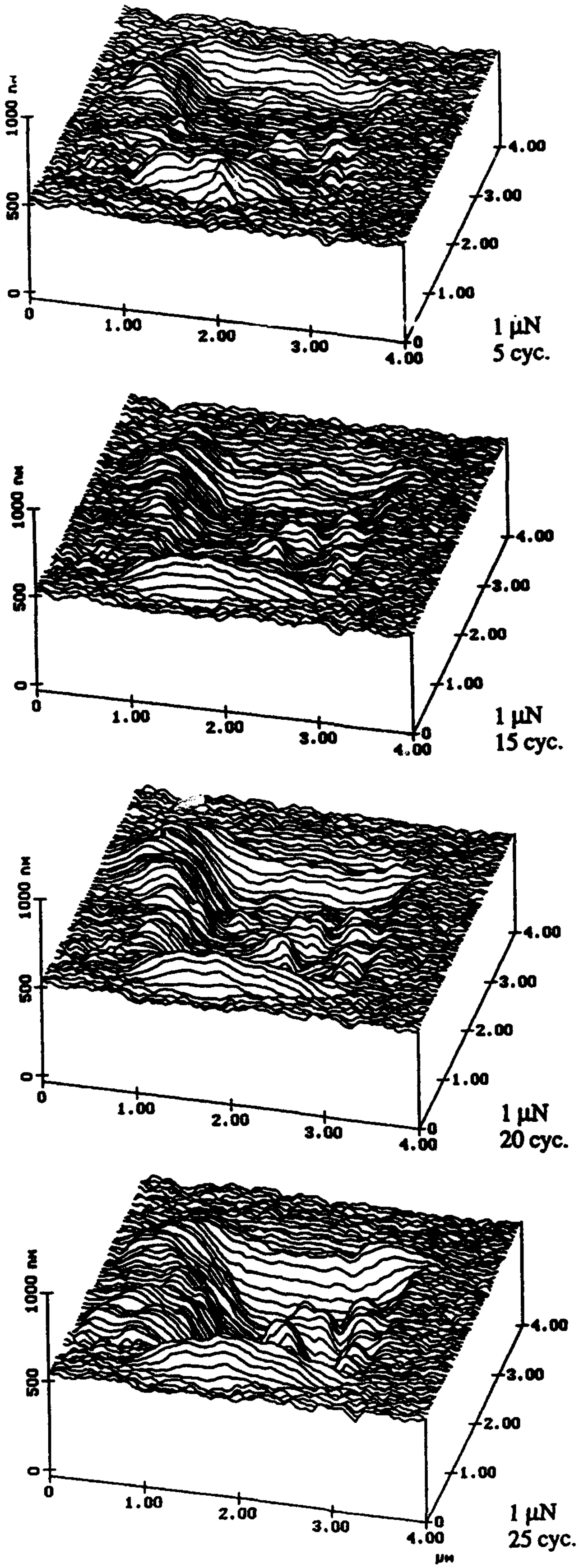

1000 nm
500
0
1.00
2.00
3.00
4.00
1 µN
5 cyc.
1 µN
15 cyc.
1 µN
20 cyc.
1 µN
25 cyc.
µm

Fig. 18

Gray scale plot

Inverted line plot

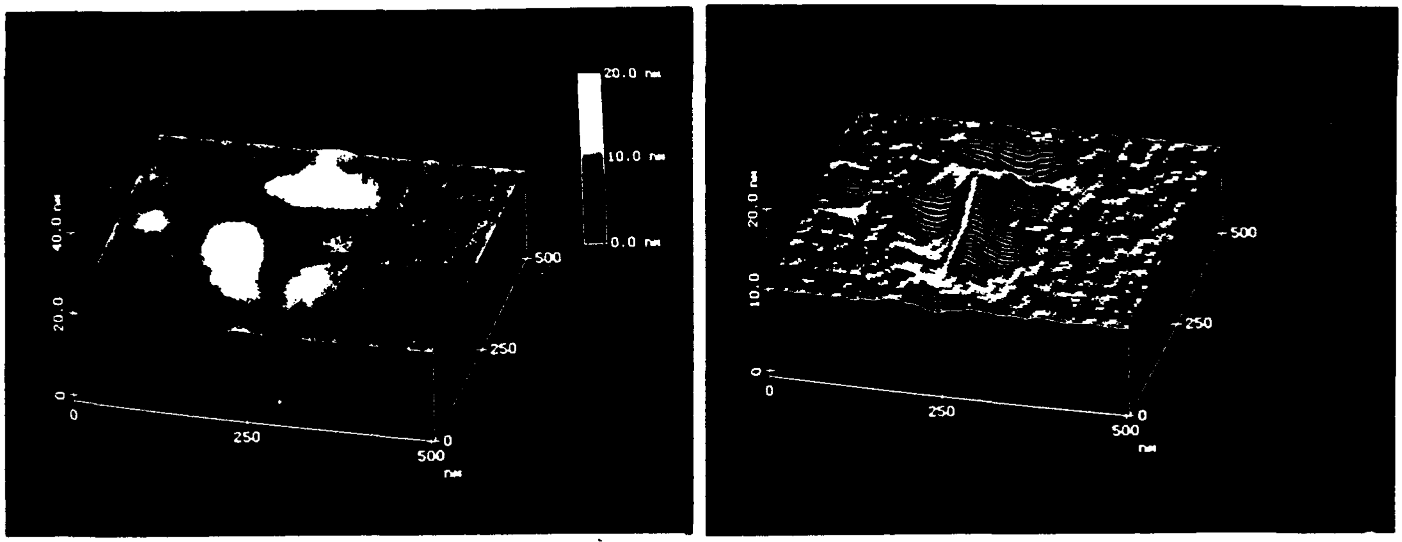

Load=70 μN, depth=3 nm, hardness=16 GPa

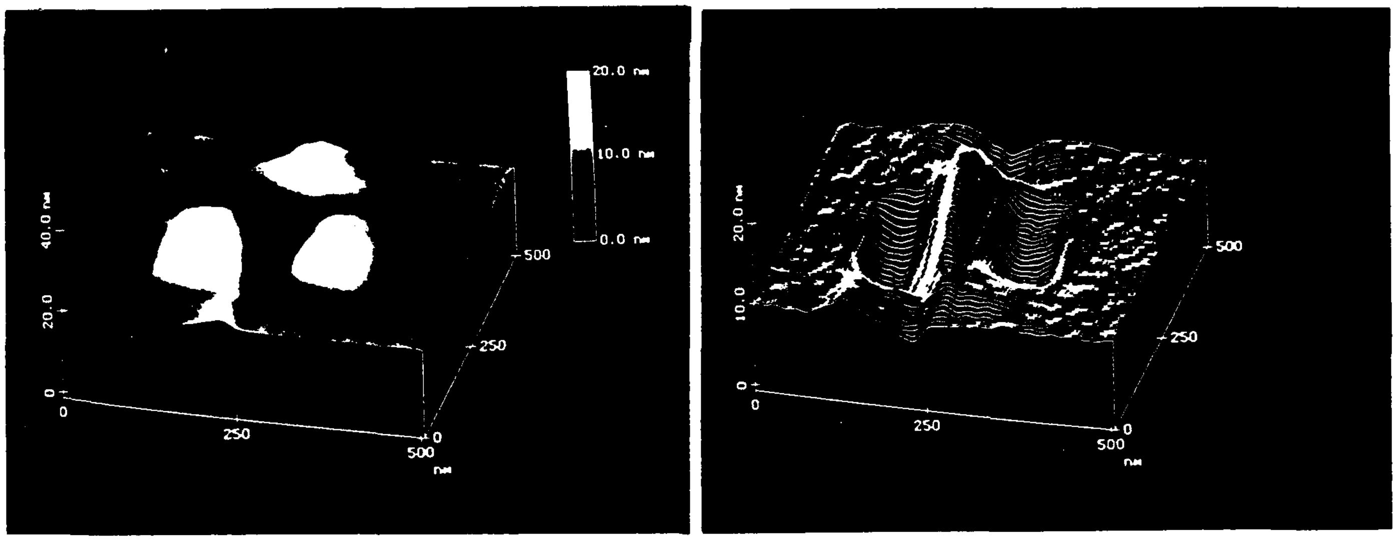

Load=100 μN, depth=7 nm, hardness=12 GPa

(a)

(b)

Fig. 19

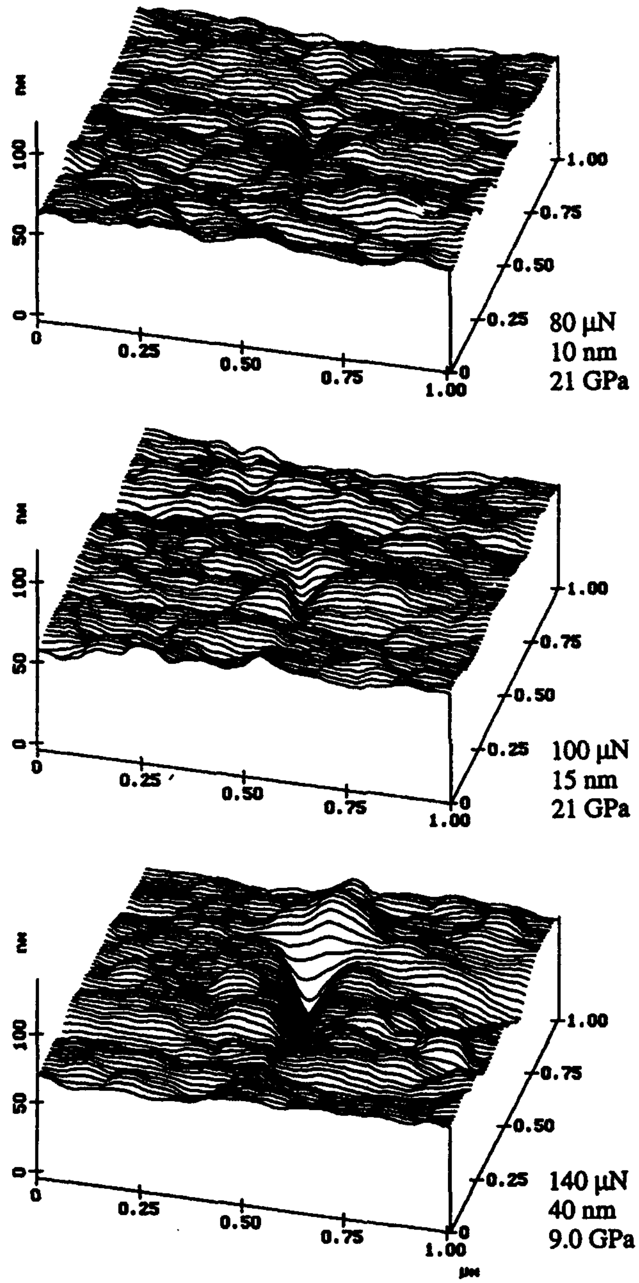
nm
0
50
100
0
0.25
0.50
0.75
1.00
80 µN
10 nm
21 GPa
100 µN
15 nm
21 GPa
140 µN
40 nm
9.0 GPa
µm

Fig. 2b

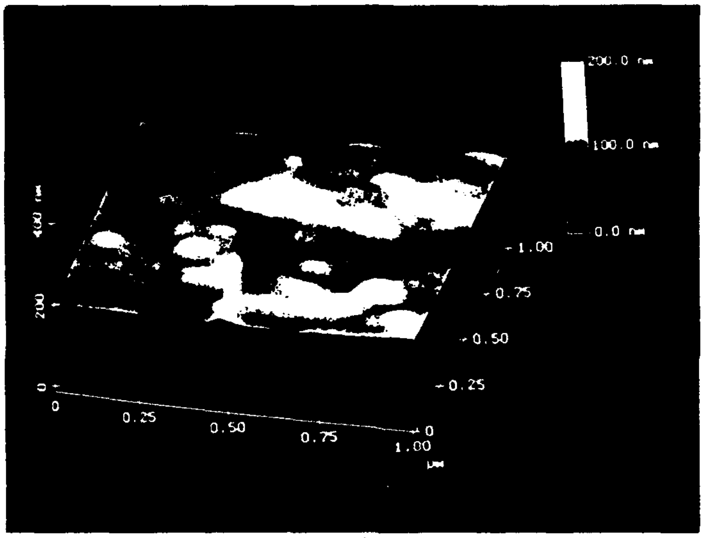
200.0 nm
100.0 nm
0.0 nm
400
200
0
0
0.25
0.50
0.75
1.00
µm
1.00
0.75
0.50
0.25
0

(a)

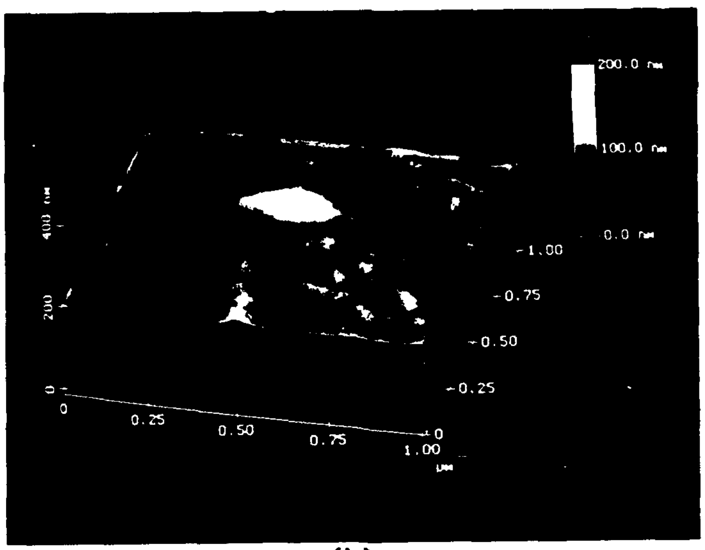
200.0 nm
100.0 nm
0.0 nm
400
200
0
0
0.25
0.50
0.75
1.00
µm
1.00
0.75
0.50
0.25
0

(b)

Fig.7

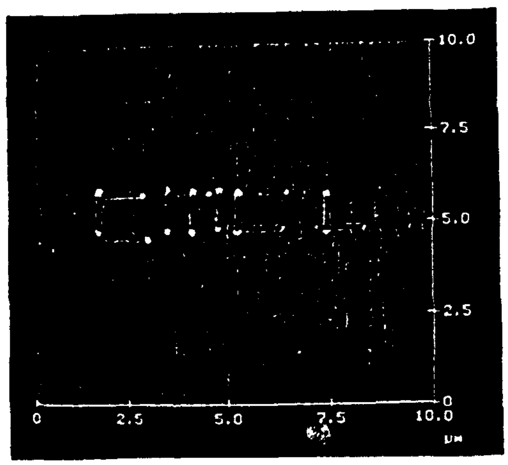

22
Fig. ~~21~~